

# European Journal of Applied Mathematics

<http://journals.cambridge.org/EJM>

Additional services for ***European Journal of Applied Mathematics***:

Email alerts: [Click here](#)

Subscriptions: [Click here](#)

Commercial reprints: [Click here](#)

Terms of use : [Click here](#)



---

## Time-reversal algorithms in viscoelastic media

HABIB AMMARI, ELIE BRETIN, JOSSELIN GARNIER and ABDUL WAHAB

European Journal of Applied Mathematics / Volume 24 / Issue 04 / August 2013, pp 565 - 600  
DOI: 10.1017/S0956792513000107, Published online: 03 April 2013

**Link to this article:** [http://journals.cambridge.org/abstract\\_S0956792513000107](http://journals.cambridge.org/abstract_S0956792513000107)

### How to cite this article:

HABIB AMMARI, ELIE BRETIN, JOSSELIN GARNIER and ABDUL WAHAB (2013). Time-reversal algorithms in viscoelastic media. *European Journal of Applied Mathematics*, 24, pp 565-600  
doi:10.1017/S0956792513000107

**Request Permissions :** [Click here](#)

# Time-reversal algorithms in viscoelastic media†

HABIB AMMARI<sup>1</sup>, ELIE BRETIN<sup>2</sup>, JOSSELIN GARNIER<sup>3</sup> and  
ABDUL WAHAB<sup>4</sup>

<sup>1</sup>*Department of Mathematics and Applications, Ecole Normale Supérieure, 45 Rue d'Ulm, 75005 Paris, France*  
email: [habib.ammari@ens.fr](mailto:habib.ammari@ens.fr)

<sup>2</sup>*Centre de Mathématiques Appliquées, CNRS UMR 7641, École Polytechnique, 91128 Palaiseau, France*  
email: [bretin@cmap.polytechnique.fr](mailto:bretin@cmap.polytechnique.fr)

<sup>3</sup>*Laboratoire de Probabilités et Modèles Aléatoires & Laboratoire Jacques-Louis Lions,*  
*Université Paris VII, 75205 Paris Cedex 13, France*

email: [garnier@math.jussieu.fr](mailto:garnier@math.jussieu.fr)  
<sup>4</sup>*Department of Mathematics, COMSATS Institute of Information Technology, G.T. Road,*  
*Wah Cantt. 47040, Pakistan*  
email: [wahab@ciitwah.edu.pk](mailto:wahab@ciitwah.edu.pk)

(Received 6 April 2012; revised 5 March 2013; accepted 5 March 2013;

first published online 3 April 2013)

In this paper we consider the problem of reconstructing sources in a homogeneous viscoelastic medium from wavefield measurements. We first present a modified time-reversal imaging algorithm based on a weighted Helmholtz decomposition and justify mathematically that it provides a better approximation than by simply time reversing the displacement field, where artifacts appear due to the coupling between the pressure and shear waves. Then we investigate the source inverse problem in an elastic attenuating medium. We provide a regularized time-reversal imaging which corrects the attenuation effect at the first order. The results of this paper yield the fundamental tools for solving imaging problems in elastic media using cross-correlation techniques.

**Key words:** Elastic wave propagation; Time-reversal algorithms; Attenuation correction; Weighted Helmholtz decomposition; Helmholtz–Kirchhoff identity

## 1 Introduction

Waves in *loss-less* media are invariant under time transformation  $t \rightarrow -t$ . This simple observation has provided very promising techniques in a variety of domains, including biomedical imaging [24], seismology [36], material analysis [41], land mine detection [39], telecommunication [37] and underwater acoustics [23]. In *time-reversal* algorithms, an *output* wave is *time-reversed* and *retransmitted* into the medium. By *time invariance* and *reciprocity* properties, the retransmitted wave retraces its path back through the medium and converges to the location of *initial sources*. This convergence of the reverted wave holds whatever is the complexity of the underlying medium, which can be homogeneous or scattering, dispersive or non-dispersive. See for instance [2, 22–28, 45 and references therein] for comprehensive details and discussions on time reversal. See also [5, 11, 19, 51] for applications of time-reversal techniques in biomedical imaging.

† This work was supported by the ERC Advanced Grant Project MULTIMOD–267184.

The robustness and simplicity of time-reversal techniques make them an ideal choice to resolve *source localization problems*. These inverse problems have been of significant interest in recent years and find numerous applications in different fields, particularly in biomedical imaging [4, 6, 8, 9, 40, 47]. If the sources are *temporally localized*, the source localization problems are actually equivalent to find *initial states* of a *system* governed by differential equations from the *observations* over some finite interval of time.

In this work, we consider the problem of reconstructing sources in a viscoelastic medium from wavefield measurements using time-reversal methods. Our motivation is the recent advances on hybrid methods in biomedical imaging exploiting elastic properties of soft tissues [30]. Examples of these hybrid methods include magnetic resonance elastography [10, 19], transient elasticity imaging [11], shear wave imaging [43] and acoustic radiation force imaging [9, 13]. The envisaged problem is quite challenging, indeed, because time reversibility of the wave equation breaks down in lossy media. Further, if not accounted for, these losses produce serious blurring in source reconstruction using classical time-reversal methods. In this paper, we use a thermo-viscous law model for the attenuation losses. We refer, for instance, to [17, 34, 35] for detailed discussions on the attenuation models in wave propagation and their causality properties.

The main contributions of this paper are twofold. We first provide a modified time-reversal imaging algorithm in non-attenuating elastic media based on a weighted Helmholtz decomposition and a Helmholtz–Kirchhoff identity for wave propagation in elastic media. Then we justify both analytically and numerically that the modified time-reversal algorithm provides a better approximation than by simply time reversing the displacement field. It has been observed that if one time-reverses the displacement field, then artifacts appear due to the coupling between the pressure and shear waves. Moreover, the focusing properties of the classical algorithm are not satisfying [19]. Using the new algorithm presented in this paper, one obtains significantly improved reconstruction and focusing properties.

Secondly, we give a regularized time-reversal imaging algorithm for source reconstruction in attenuating media and show that it leads to a first-order approximation in terms of viscosity parameters of the source term. For doing so, we express, using results from [7] based on the stationary phase theorem, the relationship between the Green tensors in attenuating and non-attenuating media. Then, with the help of a new version of Helmholtz–Kirchhoff identity in attenuating media, we prove that a regularized image of the source can be obtained. Finally, we present a variety of numerical illustrations to compare different time-reversal algorithms and to highlight the potential of our original approach.

The results of this paper yield the fundamental tools for solving imaging problems in elastic media using cross-correlation techniques. The weighted Helmholtz decomposition of the imaging functional together with the Helmholtz–Kirchhoff identities proved here are the building blocks for cross-correlation techniques in elastic media. In a forthcoming paper, the use of fundamental tools introduced in this paper for solving the problem of reconstructing spatial support of noise sources as it has been done in the acoustic case in [6] will be discussed. We also plan to develop efficient interferometric techniques based on these tools to correct for the effect of random fluctuations in the elasticity parameters on imaging and extend to the elastic case the approach investigated in [14–16].

**2 Time reversal in homogeneous elastic media without viscosity**

Let us consider the homogeneous isotropic elastic wave equation in  $\mathbb{R}^d$  with  $d = 2, 3$ :

$$\begin{cases} \frac{\partial^2 \mathbf{u}}{\partial t^2}(\mathbf{x}, t) - \mathcal{L}_{\lambda, \mu} \mathbf{u}(\mathbf{x}, t) = \frac{d\delta_0(t)}{dt} \mathbf{F}(\mathbf{x}), & (\mathbf{x}, t) \in \mathbb{R}^d \times \mathbb{R}, \\ \mathbf{u}(\mathbf{x}, t) = \frac{\partial \mathbf{u}}{\partial t}(\mathbf{x}, t) = \mathbf{0}, & \mathbf{x} \in \mathbb{R}^d, t < 0, \end{cases} \tag{2.1}$$

where

$$\mathcal{L}_{\lambda, \mu} \mathbf{u} = \mu \Delta \mathbf{u} + (\lambda + \mu) \nabla(\nabla \cdot \mathbf{u}). \tag{2.2}$$

Here  $(\lambda, \mu)$  are the Lamé coefficients of the medium and the density of the medium is equal to one. The aim in this section is to design efficient algorithms for reconstructing the compactly supported source function  $\mathbf{F}$  from the recorded data,

$$\left\{ \mathbf{g}(\mathbf{y}, t) = \mathbf{u}(\mathbf{y}, t), \mathbf{y} \in \partial\Omega, t \in [0, T] \right\}, \tag{2.3}$$

where  $\Omega$  is supposed to strictly contain the support of  $\mathbf{F}$ . We are interested in the following time-reversal functional:

$$\mathcal{I}(\mathbf{x}) = \int_0^T \mathbf{v}_s(\mathbf{x}, T) ds, \quad \mathbf{x} \in \Omega, \tag{2.4}$$

where the vector field  $\mathbf{v}_s$  is defined as the solution of

$$\begin{cases} \frac{\partial^2 \mathbf{v}_s}{\partial t^2}(\mathbf{x}, t) - \mathcal{L}_{\lambda, \mu} \mathbf{v}_s(\mathbf{x}, t) = \frac{d\delta_s(t)}{dt} \mathbf{g}(\mathbf{x}, T - s) \delta_{\partial\Omega}(\mathbf{x}), & (\mathbf{x}, t) \in \mathbb{R}^d \times \mathbb{R}, \\ \mathbf{v}_s(\mathbf{x}, t) = \frac{\partial \mathbf{v}_s}{\partial t}(\mathbf{x}, t) = \mathbf{0}, & \mathbf{x} \in \mathbb{R}^d, t < s. \end{cases} \tag{2.5}$$

Here  $\delta_{\partial\Omega}$  is the surface Dirac mass on  $\partial\Omega$  and  $\mathbf{g}$  on  $\partial\Omega \times [0, T]$  is the measured displacement field (2.3).

The time-reversal imaging functional  $\mathcal{I}$  is usually implemented to reconstruct the source distribution in an elastic medium [19, 39, 40]. It is motivated by the time reversibility property of elastic waves. In a general setting, however, it is not sure whether it provides a good reconstruction of the source distribution  $\mathbf{F}$ . Indeed the problem is that the recorded displacement field at the surface of the domain is a mixture of pressure and shear wave components. By time-reversing and back-propagating these signals as in (2.4), a blurred image is obtained due to the fact that the pressure and shear wave speeds are different.

In this work, we first present a modified time-reversal imaging functional  $\tilde{\mathcal{I}}$ , and justify mathematically that it provides a better approximation than  $\mathcal{I}$  of the source  $\mathbf{F}$ . This new functional  $\tilde{\mathcal{I}}$  can be seen as a correction based on a *weighted Helmholtz decomposition* to  $\mathcal{I}$  (which is considered as an *initial guess*). In fact, using the standard  $L^2$ -theory of the Helmholtz decomposition (see, for instance, [29]), we find in the search domain the compressional and the shear components of  $\mathcal{I}$  such that

$$\mathcal{I} = \nabla \times \psi_{\mathcal{I}} + \nabla \phi_{\mathcal{I}}. \tag{2.6}$$

Then we multiply these components with  $c_P = \sqrt{\lambda + 2\mu}$  and  $c_S = \sqrt{\mu}$ , the pressure and the shear wave speeds, respectively. Finally, we define  $\tilde{\mathcal{J}}$  by

$$\tilde{\mathcal{J}} = c_S \nabla \times \psi_{\mathcal{J}} + c_P \nabla \phi_{\mathcal{J}}. \tag{2.7}$$

We rigorously explain why should this new functional be better than the original one. We substantiate this argument with numerical illustrations.

Intuitively, since the measured data is a combination of both shear and pressure waves having different phase velocities and polarization directions, a direct time reversal of the measured data induces an interference between different backpropagating wave modes having different phases. Indeed, a back propagated P-wave produces a P-wave as well as an induced S-wave (PS-wave) in the backpropagation of P-wave. Similarly, a re-emitted S-wave produces an S-wave and an induced SP-wave. As the phases of SP- and PS-waves are not the same (due to different velocities and thus wavenumbers), the cross terms remain in time-reversal step and induce artifacts in reconstruction. The proposed re-weighting in the multi-speed case adjusts SP and PS wave phases so that the interference of such waves reduces, thereby improving the resolution in the reconstruction.

In the sequel, we define, respectively, the Helmholtz decomposition operators  $\mathcal{H}^P$  and  $\mathcal{H}^S$  by

$$\mathcal{H}^P [\mathcal{J}] := \nabla \phi_{\mathcal{J}} \quad \text{and} \quad \mathcal{H}^S [\mathcal{J}] := \nabla \times \psi_{\mathcal{J}}. \tag{2.8}$$

Actually the decomposition  $\mathcal{J} = \mathcal{H}^P [\mathcal{J}] + \mathcal{H}^S [\mathcal{J}]$  can be found by solving a weak Neumann problem in the search domain [29].

### 2.1 Time-reversal imaging analysis

In order to establish some results about time reversal using  $\mathcal{J}$  and  $\tilde{\mathcal{J}}$ , we use the following integral formulation based on the elastic Green tensor.

#### 2.1.1 Integral formulation

Let us introduce the time-dependent Green tensor  $\mathbf{G}_0(\mathbf{x}, t)$  associated to the elastic wave equation with a point source at  $\mathbf{0}$ :

$$\begin{cases} \frac{\partial^2 \mathbf{G}_0}{\partial t^2}(\mathbf{x}, t) - \mathcal{L}_{\lambda, \mu} \mathbf{G}_0(\mathbf{x}, t) = \delta_0(t) \delta_0(\mathbf{x}) \mathbf{I}, & (\mathbf{x}, t) \in \mathbb{R}^d \times \mathbb{R}, \\ \mathbf{G}_0(\mathbf{x}, t) = \frac{\partial \mathbf{G}_0}{\partial t}(\mathbf{x}, t) = \mathbf{0}, & \mathbf{x} \in \mathbb{R}^d, t < 0, \end{cases} \tag{2.9}$$

and the corresponding outgoing time-harmonic Green tensor  $\hat{\mathbf{G}}_{\omega, 0}(\mathbf{x})$  (i.e. the temporal Fourier transform of  $\mathbf{G}_0(\mathbf{x}, t)$ ) solution of

$$(\mathcal{L}_{\lambda, \mu} + \omega^2) \hat{\mathbf{G}}_{\omega, 0}(\mathbf{x}) = -\delta_0(\mathbf{x}) \mathbf{I}, \quad \mathbf{x} \in \mathbb{R}^d. \tag{2.10}$$

It can be expressed in the following form [1, 12]:

$$\hat{\mathbf{G}}_{\omega, 0}(\mathbf{x}) = \frac{1}{\mu \kappa_S^2} \left( \kappa_S^2 \hat{\mathbf{G}}_{\omega, 0}^S(\mathbf{x}) \mathbf{I} + \mathbf{D} \left( \hat{\mathbf{G}}_{\omega, 0}^S - \hat{\mathbf{G}}_{\omega, 0}^P \right) (\mathbf{x}) \right), \quad \mathbf{x} \in \mathbb{R}^d, \tag{2.11}$$

where  $\mathbf{I} = (\delta_{ij})_{i,j=1}^d$  and  $\mathbf{D} = (\frac{\partial^2}{\partial x_i \partial x_j})_{i,j=1}^d$ . The coefficients

$$\kappa_S = \frac{\omega}{\sqrt{\mu}} \quad \text{and} \quad \kappa_P = \frac{\omega}{\sqrt{\lambda + 2\mu}}$$

are the shear and the pressure wavenumbers, respectively. The function  $\hat{G}_{\omega,0}^\alpha(\mathbf{x})$  is the fundamental solution of the Helmholtz operator  $-(\Delta + \kappa_\alpha^2)$  in  $\mathbb{R}^d$  with  $\alpha = P, S$ . For example, when  $d = 3$ , we have

$$\hat{G}_{\omega,0}^\alpha(\mathbf{x}) = \frac{\exp(i\kappa_\alpha|\mathbf{x}|)}{4\pi|\mathbf{x}|}, \quad \alpha = P, S. \tag{2.12}$$

For  $T$  large enough, the functional  $\mathcal{J}(\mathbf{x})$  defined by (2.4) can be expressed in the form [5]

$$\begin{aligned} \mathcal{J}(\mathbf{x}) &= \Re e \left[ \frac{1}{2\pi} \int_{\mathbb{R}^d} \int_{\mathbb{R}} \omega^2 \left[ \int_{\partial\Omega} \hat{\mathbf{G}}_\omega(\mathbf{x}, \mathbf{y}) \overline{\hat{\mathbf{G}}_\omega(\mathbf{y}, z)} d\sigma(\mathbf{y}) \right] d\omega \mathbf{F}(z) dz \right] \\ &= \frac{1}{4\pi} \int_{\mathbb{R}^d} \int_{\mathbb{R}} \omega^2 \left[ \int_{\partial\Omega} \left[ \hat{\mathbf{G}}_\omega(\mathbf{x}, \mathbf{y}) \overline{\hat{\mathbf{G}}_\omega(\mathbf{y}, z)} + \overline{\hat{\mathbf{G}}_\omega(\mathbf{x}, \mathbf{y})} \hat{\mathbf{G}}_\omega(\mathbf{y}, z) \right] d\sigma(\mathbf{y}) \right] d\omega \mathbf{F}(z) dz, \end{aligned} \tag{2.13}$$

where we have introduced the outgoing Green tensor for a point source at  $\mathbf{y}$ :

$$\hat{\mathbf{G}}_\omega(\mathbf{x}, \mathbf{y}) = \hat{\mathbf{G}}_{\omega,0}(\mathbf{x} - \mathbf{y}). \tag{2.14}$$

We also introduce the decomposition of  $\hat{\mathbf{G}}_{\omega,0}$  into shear and compressional components as

$$\hat{\mathbf{G}}_{\omega,0}(\mathbf{x}) = \hat{\mathbf{G}}_{\omega,0}^P(\mathbf{x}) + \hat{\mathbf{G}}_{\omega,0}^S(\mathbf{x}), \tag{2.15}$$

with

$$\hat{\mathbf{G}}_{\omega,0}^P = -\frac{1}{\omega^2} \mathbf{D} \hat{\mathbf{G}}_{\omega,0}^P \quad \text{and} \quad \hat{\mathbf{G}}_{\omega,0}^S = \frac{1}{\omega^2} (\kappa_S^2 \mathbf{I} + \mathbf{D}) \hat{\mathbf{G}}_{\omega,0}^S. \tag{2.16}$$

We can extend Helmholtz operators  $\mathcal{H}^P$  and  $\mathcal{H}^S$  to tensors  $\mathbf{G}$  as follows:

$$\mathcal{H}^P[\mathbf{G}]\mathbf{p} = \mathcal{H}^P[\mathbf{G}\mathbf{p}] \quad \text{and} \quad \mathcal{H}^S[\mathbf{G}]\mathbf{p} = \mathcal{H}^S[\mathbf{G}\mathbf{p}] \quad \text{for all vectors } \mathbf{p}.$$

Note that  $\hat{\mathbf{G}}_{\omega,0}^P$  and  $\hat{\mathbf{G}}_{\omega,0}^S$  satisfy, respectively,

$$(\mathcal{L}_{\lambda,\mu} + \omega^2) \hat{\mathbf{G}}_{\omega,0}^P = \mathcal{H}^P[-\delta_0 \mathbf{I}] \quad \text{and} \quad (\mathcal{L}_{\lambda,\mu} + \omega^2) \hat{\mathbf{G}}_{\omega,0}^S = \mathcal{H}^S[-\delta_0 \mathbf{I}]. \tag{2.17}$$

Here

$$\mathcal{H}^P[-\delta_0 \mathbf{I}] = -\nabla \nabla \cdot (\mathbf{G}\mathbf{I}), \quad \mathcal{H}^S[-\delta_0 \mathbf{I}] = \nabla \times \nabla \times (\mathbf{G}\mathbf{I}),$$

and  $G(\mathbf{x}) = 1/(4\pi|\mathbf{x}|)$  for  $d = 3$  [42]. Consequently, the Helmholtz decomposition of  $\mathcal{J}$  can be derived explicitly:

$$\mathcal{J}(\mathbf{x}) = \mathcal{H}^P[\mathcal{J}](\mathbf{x}) + \mathcal{H}^S[\mathcal{J}](\mathbf{x}), \tag{2.18}$$

with

$$\begin{aligned} \mathcal{H}^P[\mathcal{J}](\mathbf{x}) &= \frac{1}{4\pi} \int_{\mathbb{R}^d} \int_{\mathbb{R}} \omega^2 \left[ \int_{\partial\Omega} \left[ \hat{\mathbf{G}}_\omega^P(\mathbf{x}, \mathbf{y}) \overline{\hat{\mathbf{G}}_\omega(\mathbf{y}, \mathbf{z})} \right. \right. \\ &\quad \left. \left. + \overline{\hat{\mathbf{G}}_\omega^P(\mathbf{x}, \mathbf{y})} \hat{\mathbf{G}}_\omega(\mathbf{y}, \mathbf{z}) \right] d\sigma(\mathbf{y}) \right] d\omega \mathbf{F}(\mathbf{z}) dz, \end{aligned}$$

and

$$\begin{aligned} \mathcal{H}^S[\mathcal{J}](\mathbf{x}) &= \frac{1}{4\pi} \int_{\mathbb{R}^d} \int_{\mathbb{R}} \omega^2 \left[ \int_{\partial\Omega} \left[ \hat{\mathbf{G}}_\omega^S(\mathbf{x}, \mathbf{y}) \overline{\hat{\mathbf{G}}_\omega(\mathbf{y}, \mathbf{z})} \right. \right. \\ &\quad \left. \left. + \overline{\hat{\mathbf{G}}_\omega^S(\mathbf{x}, \mathbf{y})} \hat{\mathbf{G}}_\omega(\mathbf{y}, \mathbf{z}) \right] d\sigma(\mathbf{y}) \right] d\omega \mathbf{F}(\mathbf{z}) dz. \end{aligned}$$

Finally, the integral formulation of the modified imaging functional  $\tilde{\mathcal{J}}$  defined by (2.7) reads

$$\tilde{\mathcal{J}}(\mathbf{x}) = \Re e \left[ \frac{1}{2\pi} \int_{\mathbb{R}^d} \int_{\mathbb{R}} \omega^2 \left[ \int_{\partial\Omega} \left[ c_S \hat{\mathbf{G}}_\omega^S(\mathbf{x}, \mathbf{y}) + c_P \hat{\mathbf{G}}_\omega^P(\mathbf{x}, \mathbf{y}) \right] \overline{\hat{\mathbf{G}}_\omega(\mathbf{y}, \mathbf{z})} d\sigma(\mathbf{y}) \right] d\omega \mathbf{F}(\mathbf{z}) dz \right]. \tag{2.19}$$

### 2.1.2 Helmholtz–Kirchhoff identity

In order to approximate the integral formulation (2.19) we use a Helmholtz–Kirchhoff identity for elastic media. Some of the results presented in this section can be found in [48,49] in the context of elastodynamic seismic interferometry. Indeed, the elastodynamic reciprocity theorems (Propositions 2.1 and 2.5) are the key ingredient to understand the relation between the cross-correlations of signals emitted by uncorrelated noise sources and the Green function between the observation points.

Let us introduce the conormal derivative  $(\partial\mathbf{u}/\partial\nu)(\mathbf{y})$ ,  $\mathbf{y} \in \partial\Omega$  of the displacement field  $\mathbf{u}$  at the surface  $\partial\Omega$  in the outward unit normal direction  $\mathbf{n}$  by

$$\frac{\partial\mathbf{u}}{\partial\nu} := \lambda(\nabla \cdot \mathbf{u})\mathbf{n} + \mu(\nabla\mathbf{u}^T + (\nabla\mathbf{u}^T)^T)\mathbf{n}, \tag{2.20}$$

where  $T$  denotes the transpose. Physically, the conormal derivative describes the surface traction associated with the displacement field  $\mathbf{u}$ . Also note that the conormal derivative tensor  $\partial\mathbf{G}/\partial\nu$  means that for all constant vectors  $\mathbf{p}$ ,

$$\left[ \frac{\partial\mathbf{G}}{\partial\nu} \right] \mathbf{p} := \frac{\partial [\mathbf{G}\mathbf{p}]}{\partial\nu}.$$

The following proposition is equivalent to [49, equation (73)]. Since our formulation is slightly different and this is the first building block of our theory, we give its proof for consistency. Moreover, elements of the proof are used in Proposition 2.2. The proof of Proposition 2.1 uses only the reciprocity relation and the divergence theorem. Consequently, Proposition 2.1 also holds in a heterogeneous medium, as shown in [49].

**Proposition 2.1** For all  $\mathbf{x}, \mathbf{z} \in \Omega$ , we have

$$\int_{\partial\Omega} \left[ \frac{\partial \hat{\mathbf{G}}_\omega(\mathbf{x}, \mathbf{y})}{\partial \mathbf{v}} \overline{\hat{\mathbf{G}}_\omega(\mathbf{y}, \mathbf{z})} - \hat{\mathbf{G}}_\omega(\mathbf{x}, \mathbf{y}) \frac{\partial \overline{\hat{\mathbf{G}}_\omega(\mathbf{y}, \mathbf{z})}}{\partial \mathbf{v}} \right] d\sigma(\mathbf{y}) = 2i \Im m\{\hat{\mathbf{G}}_\omega(\mathbf{x}, \mathbf{z})\}. \quad (2.21)$$

**Proof** By reciprocity we have

$$\hat{\mathbf{G}}_\omega(\mathbf{y}, \mathbf{x}) = [\hat{\mathbf{G}}_\omega(\mathbf{x}, \mathbf{y})]^T. \quad (2.22)$$

In addition, in the homogeneous isotropic case, we have  $\hat{\mathbf{G}}_\omega(\mathbf{y}, \mathbf{x}) = \hat{\mathbf{G}}_\omega(\mathbf{x}, \mathbf{y})$ , but we will not use this property here. Our goal is to show that for all constant vectors  $\mathbf{p}$  and  $\mathbf{q}$ , we have

$$\int_{\partial\Omega} \left[ \mathbf{q} \cdot \frac{\partial \hat{\mathbf{G}}_\omega(\mathbf{x}, \mathbf{y})}{\partial \mathbf{v}} \overline{\hat{\mathbf{G}}_\omega(\mathbf{y}, \mathbf{z})} \mathbf{p} - \mathbf{q} \cdot \hat{\mathbf{G}}_\omega(\mathbf{x}, \mathbf{y}) \frac{\partial \overline{\hat{\mathbf{G}}_\omega(\mathbf{y}, \mathbf{z})}}{\partial \mathbf{v}} \mathbf{p} \right] d\sigma(\mathbf{y}) = 2i \mathbf{q} \cdot \Im m\{\hat{\mathbf{G}}_\omega(\mathbf{x}, \mathbf{z})\} \mathbf{p}.$$

Taking scalar product of equations

$$(\mathcal{L}_{\lambda,\mu} + \omega^2) \hat{\mathbf{G}}_\omega(\mathbf{y}, \mathbf{x}) \mathbf{q} = -\delta_{\mathbf{x}}(\mathbf{y}) \mathbf{q} \quad \text{and} \quad (\mathcal{L}_{\lambda,\mu} + \omega^2) \overline{\hat{\mathbf{G}}_\omega(\mathbf{y}, \mathbf{z})} \mathbf{p} = -\delta_{\mathbf{z}}(\mathbf{y}) \mathbf{p}$$

with  $\overline{\hat{\mathbf{G}}_\omega(\mathbf{y}, \mathbf{z})} \mathbf{p}$  and  $\hat{\mathbf{G}}_\omega(\mathbf{y}, \mathbf{x}) \mathbf{q}$ , respectively, subtracting the second result from the first, and integrating in  $\mathbf{y}$  over  $\Omega$ , we obtain

$$\begin{aligned} & \int_{\Omega} \left[ (\overline{\hat{\mathbf{G}}_\omega(\mathbf{y}, \mathbf{z})} \mathbf{p}) \cdot \mathcal{L}_{\lambda,\mu}(\hat{\mathbf{G}}_\omega(\mathbf{y}, \mathbf{x}) \mathbf{q}) - \mathcal{L}_{\lambda,\mu}(\overline{\hat{\mathbf{G}}_\omega(\mathbf{y}, \mathbf{z})} \mathbf{p}) \cdot (\hat{\mathbf{G}}_\omega(\mathbf{y}, \mathbf{x}) \mathbf{q}) \right] d\mathbf{y} \\ & = \mathbf{p} \cdot (\hat{\mathbf{G}}_\omega(\mathbf{z}, \mathbf{x}) \mathbf{q}) - \mathbf{q} \cdot (\overline{\hat{\mathbf{G}}_\omega(\mathbf{x}, \mathbf{z})} \mathbf{p}) = 2i \mathbf{q} \cdot \Im m\{\hat{\mathbf{G}}_\omega(\mathbf{x}, \mathbf{z})\} \mathbf{p}. \end{aligned}$$

Using the form of the operator  $\mathcal{L}_{\lambda,\mu}$ , this gives

$$\begin{aligned} & 2i \mathbf{q} \cdot \Im m\{\hat{\mathbf{G}}_\omega(\mathbf{x}, \mathbf{z})\} \mathbf{p} \\ & = \lambda \int_{\Omega} \left[ (\overline{\hat{\mathbf{G}}_\omega(\mathbf{y}, \mathbf{z})} \mathbf{p}) \cdot \left\{ \nabla \nabla \cdot (\hat{\mathbf{G}}_\omega(\mathbf{y}, \mathbf{x}) \mathbf{q}) \right\} - (\hat{\mathbf{G}}_\omega(\mathbf{y}, \mathbf{x}) \mathbf{q}) \cdot \left\{ \nabla \nabla \cdot (\overline{\hat{\mathbf{G}}_\omega(\mathbf{y}, \mathbf{z})} \mathbf{p}) \right\} \right] d\mathbf{y} \\ & \quad + \mu \int_{\Omega} \left[ (\overline{\hat{\mathbf{G}}_\omega(\mathbf{y}, \mathbf{z})} \mathbf{p}) \cdot \left\{ (\Delta + \nabla \nabla \cdot)(\hat{\mathbf{G}}_\omega(\mathbf{y}, \mathbf{x}) \mathbf{q}) \right\} \right. \\ & \quad \left. - (\hat{\mathbf{G}}_\omega(\mathbf{y}, \mathbf{x}) \mathbf{q}) \cdot \left\{ (\Delta + \nabla \nabla \cdot)(\overline{\hat{\mathbf{G}}_\omega(\mathbf{y}, \mathbf{z})} \mathbf{p}) \right\} \right] d\mathbf{y}. \end{aligned}$$

We recall that, for two sufficiently smooth functions  $\mathbf{u}, \mathbf{v} : \mathbb{R}^d \rightarrow \mathbb{R}^d$ , we have

$$\begin{aligned} (\Delta \mathbf{u} + \nabla(\nabla \cdot \mathbf{u})) \cdot \mathbf{v} &= \nabla \cdot [(\nabla \mathbf{u}^T + (\nabla \mathbf{u}^T)^T) \mathbf{v}] - \frac{1}{2} (\nabla \mathbf{u}^T + (\nabla \mathbf{u}^T)^T) \cdot (\nabla \mathbf{v}^T + (\nabla \mathbf{v}^T)^T), \\ \nabla(\nabla \cdot \mathbf{u}) \cdot \mathbf{v} &= \nabla \cdot [(\nabla \cdot \mathbf{u}) \mathbf{v}] - (\nabla \cdot \mathbf{u})(\nabla \cdot \mathbf{v}). \end{aligned}$$



Therefore, we find

$$\begin{aligned}
 & 2iq \cdot \Im\{\hat{\mathbf{G}}_\omega(\mathbf{x}, \mathbf{z})\} \mathbf{p} \\
 &= \lambda \int_\Omega \left[ \nabla \cdot \left\{ [\nabla \cdot (\hat{\mathbf{G}}_\omega(\mathbf{y}, \mathbf{x})\mathbf{q})](\overline{\hat{\mathbf{G}}_\omega(\mathbf{y}, \mathbf{z})\mathbf{p}}) \right\} - \nabla \cdot \left\{ [\nabla \cdot (\overline{\hat{\mathbf{G}}_\omega(\mathbf{y}, \mathbf{z})\mathbf{p}})](\hat{\mathbf{G}}_\omega(\mathbf{y}, \mathbf{x})\mathbf{q}) \right\} \right] d\mathbf{y} \\
 &+ \mu \int_\Omega \left[ \nabla \cdot \left\{ \left( \nabla(\hat{\mathbf{G}}_\omega(\mathbf{y}, \mathbf{x})\mathbf{q})^T + (\nabla(\hat{\mathbf{G}}_\omega(\mathbf{y}, \mathbf{x})\mathbf{q})^T)^T \right) \overline{\hat{\mathbf{G}}_\omega(\mathbf{y}, \mathbf{z})\mathbf{p}} \right\} \right. \\
 &\left. - \nabla \cdot \left\{ \left( \overline{\hat{\mathbf{G}}_\omega(\mathbf{y}, \mathbf{z})\mathbf{p}}^T + (\nabla(\overline{\hat{\mathbf{G}}_\omega(\mathbf{y}, \mathbf{z})\mathbf{p}})^T)^T \right) \hat{\mathbf{G}}_\omega(\mathbf{y}, \mathbf{x})\mathbf{q} \right\} \right] d\mathbf{y}.
 \end{aligned}$$

Now we use divergence theorem and the definition of the conormal derivative to get

$$\begin{aligned}
 & 2iq \cdot \Im\{\hat{\mathbf{G}}_\omega(\mathbf{x}, \mathbf{z})\} \mathbf{p} \\
 &= \lambda \int_{\partial\Omega} \left[ \mathbf{n} \cdot \left\{ [\nabla \cdot (\hat{\mathbf{G}}_\omega(\mathbf{y}, \mathbf{x})\mathbf{q})](\overline{\hat{\mathbf{G}}_\omega(\mathbf{y}, \mathbf{z})\mathbf{p}}) \right\} - \mathbf{n} \cdot \left\{ [\nabla \cdot (\overline{\hat{\mathbf{G}}_\omega(\mathbf{y}, \mathbf{z})\mathbf{p}})](\hat{\mathbf{G}}_\omega(\mathbf{y}, \mathbf{x})\mathbf{q}) \right\} \right] d\sigma(\mathbf{y}) \\
 &+ \mu \int_{\partial\Omega} \left[ \mathbf{n} \cdot \left\{ \left( \nabla(\hat{\mathbf{G}}_\omega(\mathbf{y}, \mathbf{x})\mathbf{q})^T + (\nabla(\hat{\mathbf{G}}_\omega(\mathbf{y}, \mathbf{x})\mathbf{q})^T)^T \right) \overline{\hat{\mathbf{G}}_\omega(\mathbf{y}, \mathbf{z})\mathbf{p}} \right\} \right. \\
 &\left. - \mathbf{n} \cdot \left\{ \left( \nabla(\overline{\hat{\mathbf{G}}_\omega(\mathbf{y}, \mathbf{z})\mathbf{p}})^T + (\nabla(\overline{\hat{\mathbf{G}}_\omega(\mathbf{y}, \mathbf{z})\mathbf{p}})^T)^T \right) \hat{\mathbf{G}}_\omega(\mathbf{y}, \mathbf{x})\mathbf{q} \right\} \right] d\sigma(\mathbf{y}) \\
 &= \lambda \int_{\partial\Omega} \left[ (\overline{\hat{\mathbf{G}}_\omega(\mathbf{y}, \mathbf{z})\mathbf{p}}) \cdot \left\{ \nabla \cdot (\hat{\mathbf{G}}_\omega(\mathbf{y}, \mathbf{x})\mathbf{q})\mathbf{n} \right\} - (\hat{\mathbf{G}}_\omega(\mathbf{y}, \mathbf{x})\mathbf{q}) \cdot \left\{ \nabla \cdot (\overline{\hat{\mathbf{G}}_\omega(\mathbf{y}, \mathbf{z})\mathbf{p}})\mathbf{n} \right\} \right] d\sigma(\mathbf{y}) \\
 &+ \mu \int_{\partial\Omega} \left[ (\overline{\hat{\mathbf{G}}_\omega(\mathbf{y}, \mathbf{z})\mathbf{p}}) \cdot \left\{ \left( \nabla(\hat{\mathbf{G}}_\omega(\mathbf{y}, \mathbf{x})\mathbf{q})^T + (\nabla(\hat{\mathbf{G}}_\omega(\mathbf{y}, \mathbf{x})\mathbf{q})^T)^T \right) \mathbf{n} \right\} \right. \\
 &\left. - (\hat{\mathbf{G}}_\omega(\mathbf{y}, \mathbf{x})\mathbf{q}) \cdot \left\{ \left( \nabla(\overline{\hat{\mathbf{G}}_\omega(\mathbf{y}, \mathbf{z})\mathbf{p}})^T + (\nabla(\overline{\hat{\mathbf{G}}_\omega(\mathbf{y}, \mathbf{z})\mathbf{p}})^T)^T \right) \mathbf{n} \right\} \right] d\sigma(\mathbf{y}) \\
 &= \int_{\partial\Omega} \left[ (\overline{\hat{\mathbf{G}}_\omega(\mathbf{y}, \mathbf{z})\mathbf{p}}) \cdot \frac{\partial \hat{\mathbf{G}}_\omega(\mathbf{y}, \mathbf{x})\mathbf{q}}{\partial \mathbf{v}} - (\hat{\mathbf{G}}_\omega(\mathbf{y}, \mathbf{x})\mathbf{q}) \cdot \frac{\partial \overline{\hat{\mathbf{G}}_\omega(\mathbf{y}, \mathbf{z})\mathbf{p}}}{\partial \mathbf{v}} \right] d\sigma(\mathbf{y}) \\
 &= \int_{\partial\Omega} \left[ \mathbf{q} \cdot \frac{\partial \hat{\mathbf{G}}_\omega(\mathbf{x}, \mathbf{y})}{\partial \mathbf{v}} \overline{\hat{\mathbf{G}}_\omega(\mathbf{y}, \mathbf{z})\mathbf{p}} - \mathbf{q} \cdot \hat{\mathbf{G}}_\omega(\mathbf{x}, \mathbf{y}) \frac{\partial \overline{\hat{\mathbf{G}}_\omega(\mathbf{y}, \mathbf{z})\mathbf{p}}}{\partial \mathbf{v}} \right] d\sigma(\mathbf{y}),
 \end{aligned}$$

which is the desired result. Note that for establishing the last equality, we have used the reciprocity relation (2.22). □

The following proposition cannot be found in the literature, probably because its application in the context of seismic interferometry has not yet been identified. It is an important ingredient in the analysis of our improved imaging functional. Note that the proofs of Propositions 2.2 and 2.3 require the medium to be homogeneous (so that  $\mathcal{H}^S$  and  $\mathcal{H}^P$  commute with  $\mathcal{L}_{\lambda, \mu}$ ), and we cannot expect Propositions 2.2 and 2.3 to be true in a heterogeneous medium because of mode conversion between pressure and shear waves.

**Proposition 2.2** *For all  $\mathbf{x}, \mathbf{z} \in \Omega$ , we have*

$$\int_{\partial\Omega} \left[ \frac{\partial \hat{\mathbf{G}}_\omega^S(\mathbf{x}, \mathbf{y})}{\partial \mathbf{v}} \overline{\hat{\mathbf{G}}_\omega^P(\mathbf{y}, \mathbf{z})} - \hat{\mathbf{G}}_\omega^S(\mathbf{x}, \mathbf{y}) \frac{\partial \overline{\hat{\mathbf{G}}_\omega^P(\mathbf{y}, \mathbf{z})}}{\partial \mathbf{v}} \right] d\sigma(\mathbf{y}) = 0. \tag{2.23}$$

**Proof** First, we recall that  $\hat{\mathbf{G}}_\omega^P(\mathbf{y}, \mathbf{x})$  and  $\hat{\mathbf{G}}_\omega^S(\mathbf{y}, \mathbf{x})$  are solutions of (2.17). We proceed as in the proof of Proposition 2.1 to find:

$$\begin{aligned} & \int_{\partial\Omega} \left[ \frac{\partial \hat{\mathbf{G}}_\omega^S(\mathbf{x}, \mathbf{y})}{\partial \nu} \overline{\hat{\mathbf{G}}_\omega^P(\mathbf{y}, \mathbf{z})} - \hat{\mathbf{G}}_\omega^S(\mathbf{x}, \mathbf{y}) \frac{\partial \overline{\hat{\mathbf{G}}_\omega^P(\mathbf{y}, \mathbf{z})}}{\partial \nu} \right] d\sigma(\mathbf{y}) \\ &= \int_\Omega \left[ \mathcal{H}^S[-\delta_{\mathbf{x}}\mathbf{I}](\mathbf{y}) \overline{\hat{\mathbf{G}}_\omega^P(\mathbf{y}, \mathbf{z})} - \hat{\mathbf{G}}_\omega^S(\mathbf{x}, \mathbf{y}) \mathcal{H}^P[-\delta_{\mathbf{z}}\mathbf{I}](\mathbf{y}) \right] d\mathbf{y} \\ &= [\mathcal{H}^S[-\delta_0\mathbf{I}] * \overline{\hat{\mathbf{G}}_\omega^P(\cdot, \mathbf{z})}](\mathbf{x}) - [\hat{\mathbf{G}}_\omega^S(\mathbf{x}, \cdot) * \mathcal{H}^P[-\delta_0\mathbf{I}]](\mathbf{z}). \end{aligned}$$

Using the fact that  $\hat{\mathbf{G}}_\omega^P = \mathcal{H}^P[\hat{\mathbf{G}}_\omega]$  and  $\mathcal{H}^S \mathcal{H}^P = \mathcal{H}^P \mathcal{H}^S = 0$ , we get

$$\mathcal{H}^S[\mathcal{H}^S[-\delta_0\mathbf{I}] * \overline{\hat{\mathbf{G}}_\omega^P(\cdot, \mathbf{z})}] = 0 \quad \text{and} \quad \mathcal{H}^P[\mathcal{H}^S[-\delta_0\mathbf{I}] * \overline{\hat{\mathbf{G}}_\omega^P(\cdot, \mathbf{z})}] = 0.$$

Therefore, we conclude

$$[\mathcal{H}^S[-\delta_0\mathbf{I}] * \overline{\hat{\mathbf{G}}_\omega^P(\cdot, \mathbf{z})}](\mathbf{x}) = 0.$$

Similarly, we have

$$[\hat{\mathbf{G}}_\omega^S(\mathbf{x}, \cdot) * \mathcal{H}^P[-\delta_0\mathbf{I}]](\mathbf{z}) = 0,$$

which gives the desired result. □

Finally, the following proposition shows that the elastodynamic reciprocity theorem (Proposition 2.1) holds for each wave component. As it has been said before, Proposition 2.3 holds only in a homogeneous isotropic medium.

**Proposition 2.3** For all  $\mathbf{x}, \mathbf{z} \in \mathbb{R}^d$  and  $\alpha = P, S$ ,

$$\int_{\partial\Omega} \left[ \frac{\partial \hat{\mathbf{G}}_\omega^\alpha(\mathbf{x}, \mathbf{y})}{\partial \nu(\mathbf{y})} \overline{\hat{\mathbf{G}}_\omega^\alpha(\mathbf{y}, \mathbf{z})} - \hat{\mathbf{G}}_\omega^\alpha(\mathbf{x}, \mathbf{y}) \frac{\partial \overline{\hat{\mathbf{G}}_\omega^\alpha(\mathbf{y}, \mathbf{z})}}{\partial \nu(\mathbf{y})} \right] d\sigma(\mathbf{y}) = 2i\Im m\{\hat{\mathbf{G}}_\omega^\alpha(\mathbf{x}, \mathbf{z})\}. \quad (2.24)$$

**Proof** As both cases,  $\alpha = P$  and  $\alpha = S$ , are similar, we only provide a proof for  $\alpha = P$ . For  $\alpha = P$ , indeed, we have

$$\begin{aligned} & \int_{\partial\Omega} \left[ \frac{\partial \hat{\mathbf{G}}_\omega^P(\mathbf{x}, \mathbf{y})}{\partial \nu} \overline{\hat{\mathbf{G}}_\omega^P(\mathbf{y}, \mathbf{z})} - \hat{\mathbf{G}}_\omega^P(\mathbf{x}, \mathbf{y}) \frac{\partial \overline{\hat{\mathbf{G}}_\omega^P(\mathbf{y}, \mathbf{z})}}{\partial \nu} \right] d\sigma(\mathbf{y}) \\ &= [\mathcal{H}^P[-\delta_0\mathbf{I}] * \overline{\hat{\mathbf{G}}_\omega^P(\cdot, \mathbf{z})}](\mathbf{x}) - [\hat{\mathbf{G}}_\omega^P(\mathbf{x}, \cdot) * \mathcal{H}^P[-\delta_0\mathbf{I}]](\mathbf{z}). \end{aligned}$$

Using the fact that  $\hat{\mathbf{G}}_\omega^P(\mathbf{y}, \mathbf{z}) = \hat{\mathbf{G}}_{\omega,0}^P(\mathbf{y} - \mathbf{z}) = \hat{\mathbf{G}}_{\omega,0}^P(\mathbf{z} - \mathbf{y})$ , we can write

$$[\mathcal{H}^P[-\delta_0\mathbf{I}] * \overline{\hat{\mathbf{G}}_\omega^P(\cdot, \mathbf{z})}](\mathbf{x}) = [\mathcal{H}^P[-\delta_0\mathbf{I}] * \overline{\hat{\mathbf{G}}_{\omega,0}^P(\cdot)}](\mathbf{x} - \mathbf{z}),$$

and

$$[\hat{\mathbf{G}}_\omega^P(\mathbf{x}, \cdot) * \mathcal{H}^P[-\delta_0\mathbf{I}]](\mathbf{z}) = [\hat{\mathbf{G}}_{\omega,0}^P(\cdot) * \mathcal{H}^P[-\delta_0\mathbf{I}]](\mathbf{z} - \mathbf{x}) = [\mathcal{H}^P[-\delta_0\mathbf{I}] * \overline{\hat{\mathbf{G}}_{\omega,0}^P(\cdot)}](\mathbf{x} - \mathbf{z}).$$

Therefore,

$$\int_{\partial\Omega} \left[ \frac{\partial \hat{\mathbf{G}}_{\omega}^P(\mathbf{x}, \mathbf{y})}{\partial \nu} \overline{\hat{\mathbf{G}}_{\omega}^P(\mathbf{y}, \mathbf{z})} - \hat{\mathbf{G}}_{\omega}^P(\mathbf{x}, \mathbf{y}) \frac{\partial \overline{\hat{\mathbf{G}}_{\omega}^P(\mathbf{y}, \mathbf{z})}}{\partial \nu} \right] d\sigma(\mathbf{y}) = \mathcal{H}^P \left[ 2i\Im m\{\hat{\mathbf{G}}_{\omega}^P(\mathbf{x}, \mathbf{z})\} \right] = 2i\Im m\{\hat{\mathbf{G}}_{\omega}^P(\mathbf{x}, \mathbf{z})\},$$

where the last equality results from the fact that  $\mathcal{H}^S \mathcal{H}^P = 0$ . □

### 2.1.3 Approximation of the conormal derivative

In this section we derive an approximation of the conormal derivative  $(\partial \hat{\mathbf{G}}_{\omega} / \partial \nu)(\mathbf{x}, \mathbf{y})$ ,  $\mathbf{y} \in \partial\Omega$ ,  $\mathbf{x} \in \Omega$ . In general, this approximation involves the angles between the pressure and shear rays and the normal on  $\partial\Omega$ . This approximation becomes simple when  $\Omega$  is a ball with very large radius, since in this case all rays are normal to  $\partial\Omega$  (Proposition 2.4). It allows us to use a simplified version of the Helmholtz–Kirchhoff identity to analyse the imaging functional  $\tilde{\mathcal{J}}$  when  $\Omega$  is a ball with large radius (Proposition 2.5).

**Proposition 2.4** *If  $\mathbf{n}(\mathbf{y}) = \widehat{\mathbf{y} - \mathbf{x}}$  and  $|\mathbf{x} - \mathbf{y}| \gg 1$ , then, for  $\alpha = P, S$ ,*

$$\frac{\partial \hat{\mathbf{G}}_{\omega}^{\alpha}(\mathbf{x}, \mathbf{y})}{\partial \nu(\mathbf{y})} = i\omega c_{\alpha} \hat{\mathbf{G}}_{\omega}^{\alpha}(\mathbf{x}, \mathbf{y}) + o\left(\frac{1}{|\mathbf{x} - \mathbf{y}|^{(d-1)/2}}\right). \tag{2.25}$$

**Proof** Here we only prove the proposition for  $d = 3$ . The case  $d = 2$  follows from exactly the same arguments. Moreover, it is enough to show that for all constant vectors  $\mathbf{q}$ ,

$$\frac{\partial \hat{\mathbf{G}}_{\omega}^P(\mathbf{x}, \mathbf{y})\mathbf{q}}{\partial \nu(\mathbf{y})} = i\omega c_P \hat{\mathbf{G}}_{\omega}^P(\mathbf{x}, \mathbf{y})\mathbf{q} + o\left(\frac{1}{|\mathbf{x} - \mathbf{y}|}\right)$$

and

$$\frac{\partial \hat{\mathbf{G}}_{\omega}^S(\mathbf{x}, \mathbf{y})\mathbf{q}}{\partial \nu(\mathbf{y})} = i\omega c_S \hat{\mathbf{G}}_{\omega}^S(\mathbf{x}, \mathbf{y})\mathbf{q} + o\left(\frac{1}{|\mathbf{x} - \mathbf{y}|}\right).$$

*Pressure component:* Recall that

$$\hat{\mathbf{G}}_{\omega}^P(\mathbf{x}, \mathbf{y}) = -\frac{1}{\omega^2} \mathbf{D}\hat{\mathbf{G}}_{\omega}^P(\mathbf{x}, \mathbf{y}) = \frac{1}{c_P^2} \hat{\mathbf{G}}_{\omega}^P(\mathbf{x}, \mathbf{y}) \widehat{\mathbf{y} - \mathbf{x}} \otimes \widehat{\mathbf{y} - \mathbf{x}} + o\left(\frac{1}{|\mathbf{x} - \mathbf{y}|}\right),$$

with  $\hat{\mathbf{G}}_{\omega}^P(\mathbf{x}, \mathbf{y}) = \hat{\mathbf{G}}_{\omega,0}^P(\mathbf{x} - \mathbf{y})$  and  $\hat{\mathbf{G}}_{\omega,0}^P$  given by (2.12), so we have

$$\hat{\mathbf{G}}_{\omega}^P(\mathbf{x}, \mathbf{y})\mathbf{q} = \frac{1}{c_P^2} \hat{\mathbf{G}}_{\omega}^P(\mathbf{x}, \mathbf{y}) (\widehat{\mathbf{y} - \mathbf{x}} \cdot \mathbf{q}) \widehat{\mathbf{y} - \mathbf{x}} + o\left(\frac{1}{|\mathbf{x} - \mathbf{y}|}\right).$$

Therefore,

$$\begin{aligned} \frac{\partial \hat{\mathbf{G}}_\omega^P(\mathbf{x}, \mathbf{y})\mathbf{q}}{\partial v(\mathbf{y})} &= \lambda \nabla_{\mathbf{y}} \cdot \left( \hat{\mathbf{G}}_\omega^P(\mathbf{x}, \mathbf{y})\mathbf{q} \right) \mathbf{n}(\mathbf{y}) + \mu \left[ \nabla_{\mathbf{y}}(\hat{\mathbf{G}}_\omega^P(\mathbf{x}, \mathbf{y})\mathbf{q})^T + (\nabla_{\mathbf{y}}(\hat{\mathbf{G}}_\omega^P(\mathbf{x}, \mathbf{y})\mathbf{q})^T)^T \right] \mathbf{n}(\mathbf{y}) \\ &= \frac{\widehat{\mathbf{y}} - \widehat{\mathbf{x}} \cdot \mathbf{q}}{c_P^3} i\omega \hat{\mathbf{G}}_\omega^P(\mathbf{x}, \mathbf{y}) \left[ \lambda \widehat{\mathbf{y}} - \widehat{\mathbf{x}} \cdot \widehat{\mathbf{y}} - \widehat{\mathbf{x}} \mathbf{n} + 2\mu(\widehat{\mathbf{y}} - \widehat{\mathbf{x}} \otimes \widehat{\mathbf{y}} - \widehat{\mathbf{x}})\mathbf{n} \right] + o\left(\frac{1}{|\mathbf{y} - \mathbf{x}|}\right) \\ &= \frac{\widehat{\mathbf{y}} - \widehat{\mathbf{x}} \cdot \mathbf{q}}{c_P^3} i\omega \hat{\mathbf{G}}_\omega^P(\mathbf{x}, \mathbf{y}) \left[ \lambda \mathbf{n} + 2\mu(\widehat{\mathbf{y}} - \widehat{\mathbf{x}} \cdot \mathbf{n})\widehat{\mathbf{y}} - \widehat{\mathbf{x}} \right] + o\left(\frac{1}{|\mathbf{y} - \mathbf{x}|}\right) \\ &= \frac{\widehat{\mathbf{y}} - \widehat{\mathbf{x}} \cdot \mathbf{q}}{c_P^3} i\omega \hat{\mathbf{G}}_\omega^P(\mathbf{x}, \mathbf{y}) \left[ \lambda(\mathbf{n} - \widehat{\mathbf{y}} - \widehat{\mathbf{x}}) + 2\mu(\widehat{\mathbf{y}} - \widehat{\mathbf{x}} \cdot \mathbf{n} - 1)\widehat{\mathbf{y}} - \widehat{\mathbf{x}} \right] \\ &\quad + i\omega c_P \hat{\mathbf{G}}_\omega^P(\mathbf{x}, \mathbf{y})\mathbf{q} + o\left(\frac{1}{|\mathbf{y} - \mathbf{x}|}\right). \end{aligned}$$

In particular, when  $\mathbf{n}(\mathbf{y}) = \widehat{\mathbf{y}} - \widehat{\mathbf{x}}$ , we have

$$\frac{\partial \hat{\mathbf{G}}_\omega^P(\mathbf{x}, \mathbf{y})\mathbf{q}}{\partial v(\mathbf{y})} = i\omega c_P \hat{\mathbf{G}}_\omega^P(\mathbf{x}, \mathbf{y})\mathbf{q} + o\left(\frac{1}{|\mathbf{y} - \mathbf{x}|}\right).$$

Shear components: As

$$\hat{\mathbf{G}}_\omega^S(\mathbf{x}, \mathbf{y}) = \frac{1}{\omega^2} (\kappa_S^2 \mathbf{I} + \mathbf{D}) \hat{\mathbf{G}}_\omega^S(\mathbf{x}, \mathbf{y}) = \frac{1}{c_S^2} \hat{\mathbf{G}}_\omega^S(\mathbf{x}, \mathbf{y}) (\mathbf{I} - \widehat{\mathbf{y}} - \widehat{\mathbf{x}} \otimes \widehat{\mathbf{y}} - \widehat{\mathbf{x}}) + o\left(\frac{1}{|\mathbf{x} - \mathbf{y}|}\right),$$

we have

$$\hat{\mathbf{G}}_\omega^S(\mathbf{x}, \mathbf{y})\mathbf{q} = \frac{1}{c_S^2} \hat{\mathbf{G}}_\omega^S(\mathbf{x}, \mathbf{y}) \left( \mathbf{q} - (\widehat{\mathbf{y}} - \widehat{\mathbf{x}} \cdot \mathbf{q})\widehat{\mathbf{y}} - \widehat{\mathbf{x}} \right) + o\left(\frac{1}{|\mathbf{x} - \mathbf{y}|}\right).$$

The conormal derivative is

$$\frac{\partial \hat{\mathbf{G}}_\omega^S(\mathbf{x}, \mathbf{y})\mathbf{q}}{\partial v(\mathbf{y})} = \lambda \nabla_{\mathbf{y}} \cdot \left( \hat{\mathbf{G}}_\omega^S(\mathbf{x}, \mathbf{y})\mathbf{q} \right) \mathbf{n}(\mathbf{y}) + \mu \left[ \nabla_{\mathbf{y}}(\hat{\mathbf{G}}_\omega^S(\mathbf{x}, \mathbf{y})\mathbf{q})^T + (\nabla_{\mathbf{y}}(\hat{\mathbf{G}}_\omega^S(\mathbf{x}, \mathbf{y})\mathbf{q})^T)^T \right] \mathbf{n}(\mathbf{y}).$$

Now, remark that

$$\begin{aligned} \lambda \nabla_{\mathbf{y}} \cdot \left( \hat{\mathbf{G}}_\omega^S(\mathbf{x}, \mathbf{y})\mathbf{q} \right) \mathbf{n}(\mathbf{y}) &= \lambda \frac{i\omega}{c_S^2} \hat{\mathbf{G}}_\omega^S(\mathbf{x}, \mathbf{y}) \left[ (\mathbf{q} - (\widehat{\mathbf{y}} - \widehat{\mathbf{x}} \cdot \mathbf{q})\widehat{\mathbf{y}} - \widehat{\mathbf{x}}) \cdot \widehat{\mathbf{y}} - \widehat{\mathbf{x}} \right] \mathbf{n} + o\left(\frac{1}{|\mathbf{x} - \mathbf{y}|}\right) \\ &= o\left(\frac{1}{|\mathbf{x} - \mathbf{y}|}\right), \end{aligned}$$

and

$$\begin{aligned} & \mu \left[ \nabla(\widehat{\mathbf{G}}_\omega^S(\mathbf{x}, \mathbf{y})\mathbf{q})^T + (\nabla(\widehat{\mathbf{G}}_\omega^S(\mathbf{x}, \mathbf{y})\mathbf{q})^T)^T \right] \mathbf{n} \\ &= \mu \frac{i\omega}{c_S^3} \widehat{\mathbf{G}}_\omega^S(\mathbf{x}, \mathbf{y}) \left[ \mathbf{q} \otimes \widehat{\mathbf{y}} - \widehat{\mathbf{x}} + \widehat{\mathbf{y}} - \widehat{\mathbf{x}} \otimes \mathbf{q} - 2(\widehat{\mathbf{y}} - \widehat{\mathbf{x}} \cdot \mathbf{q}) \widehat{\mathbf{y}} - \widehat{\mathbf{x}} \otimes \widehat{\mathbf{y}} - \widehat{\mathbf{x}} \right] \mathbf{n} + o\left(\frac{1}{|\mathbf{x} - \mathbf{y}|}\right) \\ &= \mu \frac{i\omega}{c_S^3} \widehat{\mathbf{G}}_\omega^S(\mathbf{x}, \mathbf{y}) \left[ (\widehat{\mathbf{y}} - \widehat{\mathbf{x}} \cdot \mathbf{n})\mathbf{q} + (\mathbf{q} \cdot \mathbf{n})\widehat{\mathbf{y}} - \widehat{\mathbf{x}} - 2(\widehat{\mathbf{y}} - \widehat{\mathbf{x}} \cdot \mathbf{q})(\widehat{\mathbf{y}} - \widehat{\mathbf{x}} \cdot \mathbf{n})\widehat{\mathbf{y}} - \widehat{\mathbf{x}} \right] \\ & \quad + o\left(\frac{1}{|\mathbf{x} - \mathbf{y}|}\right) = \mu \frac{i\omega}{c_S^3} \widehat{\mathbf{G}}_\omega^S(\mathbf{x}, \mathbf{y}) \left[ (\widehat{\mathbf{y}} - \widehat{\mathbf{x}} \cdot \mathbf{n}) - 1 \right] \left[ \mathbf{q} - (\widehat{\mathbf{y}} - \widehat{\mathbf{x}} \cdot \mathbf{q})\widehat{\mathbf{y}} - \widehat{\mathbf{x}} \right] \\ & \quad + \mu \frac{i\omega}{c_S^3} \widehat{\mathbf{G}}_\omega^S(\mathbf{x}, \mathbf{y}) \left[ (\mathbf{q} \cdot \mathbf{n} - (\widehat{\mathbf{y}} - \widehat{\mathbf{x}} \cdot \mathbf{q})(\widehat{\mathbf{y}} - \widehat{\mathbf{x}} \cdot \mathbf{n}))\widehat{\mathbf{y}} - \widehat{\mathbf{x}} \right] + i\omega c_S \widehat{\mathbf{G}}_\omega^S(\mathbf{x}, \mathbf{y})\mathbf{q} \\ & \quad + o\left(\frac{1}{|\mathbf{x} - \mathbf{y}|}\right). \end{aligned}$$

In particular, when  $\mathbf{n}(\mathbf{y}) = \widehat{\mathbf{y}} - \widehat{\mathbf{x}}$ , we have

$$\frac{\partial \widehat{\mathbf{G}}_\omega^S(\mathbf{x}, \mathbf{y})\mathbf{q}}{\partial v(\mathbf{y})} = i\omega c_S \widehat{\mathbf{G}}_\omega^S(\mathbf{x}, \mathbf{y})\mathbf{q} + o\left(\frac{1}{|\mathbf{y} - \mathbf{x}|}\right).$$

□

The following is a direct consequence of Propositions 2.2, 2.3 and 2.4.

**Proposition 2.5** *Let  $\Omega \subset \mathbb{R}^d$  be a ball with large radius  $R$ . Then, for all  $\mathbf{x}, \mathbf{z} \in \mathbb{R}^d$ , we have*

$$\lim_{R \rightarrow +\infty} \int_{\partial\Omega} \widehat{\mathbf{G}}_\omega^\alpha(\mathbf{x}, \mathbf{y}) \overline{\widehat{\mathbf{G}}_\omega^\alpha(\mathbf{y}, \mathbf{z})} d\sigma(\mathbf{y}) = \frac{1}{\omega c_\alpha} \Im m\{\widehat{\mathbf{G}}_\omega^\alpha(\mathbf{x}, \mathbf{z})\}, \quad \alpha = P, S, \tag{2.26}$$

$$\lim_{R \rightarrow +\infty} \int_{\partial\Omega} \widehat{\mathbf{G}}_\omega^S(\mathbf{x}, \mathbf{y}) \overline{\widehat{\mathbf{G}}_\omega^P(\mathbf{y}, \mathbf{z})} d\sigma(\mathbf{y}) = 0. \tag{2.27}$$

### 2.1.4 Analysis of the imaging functional $\tilde{\mathcal{I}}$

In this section, we assume that  $\Omega$  is a ball of radius  $R$  in  $\mathbb{R}^d$  and that the support,  $\text{supp}\{\mathbf{F}\}$ , of  $\mathbf{F}$  is sufficiently localized at the centre of  $\Omega$  so that for all  $\mathbf{x} \in \text{supp}\{\mathbf{F}\}$  and for all  $\mathbf{y} \in \partial\Omega$

$$\widehat{\mathbf{y}} - \widehat{\mathbf{x}} = \mathbf{n}(\mathbf{y}) + o\left(\frac{1}{|\mathbf{y} - \mathbf{x}|^{(d-1)/2}}\right).$$

Then we have the following theorem.

**Theorem 2.6** *Let  $\mathbf{x} \in \Omega$  be sufficiently far from the boundary  $\partial\Omega$  (with respect to wavelenghts) and  $\tilde{\mathcal{I}}$  be defined by (2.7). Then,*

$$\tilde{\mathcal{I}}(\mathbf{x}) \simeq \mathbf{F}(\mathbf{x}). \tag{2.28}$$

**Proof** From (2.19) we have

$$\tilde{\mathcal{I}}(\mathbf{x}) = \frac{1}{4\pi} \int_{\mathbb{R}^d} \int_{\mathbb{R}} \omega^2 \left[ \int_{\partial\Omega} \tilde{\hat{\mathbf{G}}}_\omega(\mathbf{x}, \mathbf{y}) \overline{\hat{\mathbf{G}}_\omega(\mathbf{y}, \mathbf{z})} + \overline{\tilde{\hat{\mathbf{G}}}_\omega(\mathbf{x}, \mathbf{y})} \hat{\mathbf{G}}_\omega(\mathbf{y}, \mathbf{z}) d\sigma(\mathbf{y}) \right] d\omega \mathbf{F}(\mathbf{z}) dz,$$

where

$$\tilde{\hat{\mathbf{G}}}_\omega(\mathbf{x}, \mathbf{y}) = c_S \hat{\mathbf{G}}_\omega^S(\mathbf{x}, \mathbf{y}) + c_P \hat{\mathbf{G}}_\omega^P(\mathbf{x}, \mathbf{y}).$$

Proposition 2.5 allows us to write

$$\begin{aligned} \tilde{\mathcal{I}}(\mathbf{x}) &\simeq \frac{1}{4\pi} \int_{\mathbb{R}^d} \int_{\mathbb{R}} \omega^2 \left[ \int_{\partial\Omega} \tilde{\hat{\mathbf{G}}}_\omega(\mathbf{x}, \mathbf{y}) \overline{\hat{\mathbf{G}}_\omega(\mathbf{y}, \mathbf{z})} + \overline{\hat{\mathbf{G}}_\omega(\mathbf{x}, \mathbf{y})} \tilde{\hat{\mathbf{G}}}_\omega(\mathbf{y}, \mathbf{z}) d\sigma(\mathbf{y}) \right] d\omega \mathbf{F}(\mathbf{z}) dz \\ &\simeq \frac{1}{4\pi} \int_{\mathbb{R}^d} \int_{\mathbb{R}} \omega^2 \left[ \int_{\partial\Omega} \tilde{\hat{\mathbf{G}}}_\omega(\mathbf{x}, \mathbf{y}) \overline{\hat{\mathbf{G}}_\omega(\mathbf{y}, \mathbf{z})} + \hat{\mathbf{G}}_\omega(\mathbf{x}, \mathbf{y}) \overline{\tilde{\hat{\mathbf{G}}}_\omega(\mathbf{y}, \mathbf{z})} d\sigma(\mathbf{y}) \right] d\omega \mathbf{F}(\mathbf{z}) dz. \end{aligned}$$

Propositions 2.4 and 2.1 then give

$$\begin{aligned} \tilde{\mathcal{I}}(\mathbf{x}) &\simeq \frac{1}{4\pi} \int_{\mathbb{R}^d} \int_{\mathbb{R}} -i\omega \left[ \frac{\partial \hat{\mathbf{G}}_\omega(\mathbf{x}, \mathbf{y})}{\partial \nu} \overline{\hat{\mathbf{G}}_\omega(\mathbf{y}, \mathbf{z})} - \hat{\mathbf{G}}_\omega(\mathbf{x}, \mathbf{y}) \frac{\partial \overline{\hat{\mathbf{G}}_\omega(\mathbf{y}, \mathbf{z})}}{\partial \nu} \right] d\omega \mathbf{F}(\mathbf{z}) dz \\ &\simeq \frac{1}{2\pi} \int_{\mathbb{R}^d} \int_{\mathbb{R}} \omega \Im m \left[ \hat{\mathbf{G}}_\omega(\mathbf{x}, \mathbf{z}) \right] d\omega \mathbf{F}(\mathbf{z}) dz = \mathbf{F}(\mathbf{x}). \end{aligned}$$

The last equality results from the identity

$$\frac{1}{2\pi} \int_{\mathbb{R}} -i\omega \hat{\mathbf{G}}_\omega(\mathbf{x}, \mathbf{z}) d\omega = \delta_{\mathbf{x}}(\mathbf{z}) \mathbf{I},$$

which comes from the integration of the time-dependent version of (2.10) between  $t = 0^-$  and  $t = 0^+$ .  $\square$

**Remark 2.7** If the unweighted time-reversal imaging functional  $\mathcal{I}$  is used instead of  $\tilde{\mathcal{I}}$ , then crossed terms remain. Using the same arguments as above, we find

$$\begin{aligned} \mathcal{I}(\mathbf{x}) &\simeq \frac{c_S + c_P}{c_S c_P} \frac{1}{4\pi} \int_{\mathbb{R}^d} \int_{\mathbb{R}} \omega \Im m \left[ (\hat{\mathbf{G}}_\omega^P + \hat{\mathbf{G}}_\omega^S)(\mathbf{x}, \mathbf{z}) \right] d\omega \mathbf{F}(\mathbf{z}) dz \\ &\quad + \frac{c_S - c_P}{c_S c_P} \frac{1}{4\pi} \int_{\mathbb{R}^d} \int_{\mathbb{R}} \omega \Im m \left[ (\hat{\mathbf{G}}_\omega^P - \hat{\mathbf{G}}_\omega^S)(\mathbf{x}, \mathbf{z}) \right] d\omega \mathbf{F}(\mathbf{z}) dz \\ &\simeq \frac{c_S + c_P}{2c_S c_P} \mathbf{F}(\mathbf{x}) + \frac{c_S - c_P}{2c_S c_P} \int_{\mathbb{R}^d} \mathbf{B}(\mathbf{x}, \mathbf{z}) \mathbf{F}(\mathbf{z}) dz, \end{aligned} \quad (2.29)$$

where

$$\mathbf{B}(\mathbf{x}, \mathbf{z}) = \frac{1}{2\pi} \int_{\mathbb{R}} \omega \Im m \left[ (\hat{\mathbf{G}}_\omega^P - \hat{\mathbf{G}}_\omega^S)(\mathbf{x}, \mathbf{z}) \right] d\omega \quad (2.30)$$

is the operator that describes the error in the reconstruction of the source  $\mathbf{F}$  obtained with  $\mathcal{I}$  when  $c_S \neq c_P$ . In particular, the operator  $\mathbf{B}$  is not diagonal, which means that the reconstruction mixes the components of  $\mathbf{F}$ .

### 2.2 Numerical simulations

In this section we present numerical illustrations and describe our algorithms for numerical resolution of the source problem to show that  $\tilde{\mathcal{I}}$  provides a better reconstruction than  $\mathcal{I}$ .

#### 2.2.1 Description of the algorithm

Let us describe the algorithm we used for the numerical resolution of the elastic wave equation in 2D:

$$\begin{cases} \frac{\partial^2 \mathbf{u}}{\partial t^2}(\mathbf{x}, t) = [\mu \Delta \mathbf{u} + (\lambda + \mu) \nabla(\nabla \cdot \mathbf{u})](\mathbf{x}, t), & (\mathbf{x}, t) \in \mathbb{R}^2 \times \mathbb{R}, \\ \mathbf{u}(\mathbf{x}, 0) = \mathbf{F}(\mathbf{x}) \quad \text{and} \quad \frac{\partial \mathbf{u}}{\partial t}(\mathbf{x}, 0) = \mathbf{0}. \end{cases} \tag{2.31}$$

This equation is computed in the box  $Q = [-L/2, L/2]^2$  such that  $\Omega \subset Q$  with periodic boundary conditions. We use a *splitting spectral Fourier* approach [18] coupled with a perfectly matched layer (PML) technique (see, for instance, [21, 31 and the references therein]) to simulate a free outgoing interface on  $\partial Q$ . The PML technique is implemented by adding a penalization term  $q \partial_t \mathbf{u}$  to the elastic wave equation in  $Q$ . The penalization coefficient  $q$  is supported in a neighbourhood of the boundary  $\partial Q$ . Moreover, it is a smooth positive function of the distance to  $\partial Q$  and grows exponentially. To solve the equation  $\partial_t^2 \mathbf{u} - \mathcal{L}_{\lambda, \mu} \mathbf{u} + q \partial_t \mathbf{u} = \mathbf{0}$  in  $Q$  with periodic boundary conditions, we use a splitting spectral Fourier approach. We first solve the equation  $\partial_t^2 \mathbf{u} - \mathcal{L}_{\lambda, \mu} \mathbf{u} = \mathbf{0}$  in the spatial Fourier domain and then treat the ordinary differential equation  $\partial_t^2 \mathbf{u} + q \partial_t \mathbf{u} = \mathbf{0}$  in the spatial domain.

In order to solve the elastic wave equation,  $\partial_t^2 \mathbf{u} - \mathcal{L}_{\lambda, \mu} \mathbf{u} = \mathbf{0}$  in the spatial Fourier domain, we note that it can be rewritten as a first-order partial differential equation:

$$\partial_t \mathbf{P} = \mathbf{A} \mathbf{P} + \mathbf{B} \mathbf{P},$$

where, with the notation  $\mathbf{u} = (u_1, u_2)$  and  $\mathbf{x} = (x_1, x_2)$ ,

$$\mathbf{P} = \begin{pmatrix} u_1 \\ \partial_t u_1 \\ u_2 \\ \partial_t u_2 \end{pmatrix}, \quad \mathbf{A} = \begin{pmatrix} 0 & 1 & 0 & 0 \\ (\lambda + 2\mu) \partial_{x_1}^2 + \mu \partial_{x_2}^2 & 0 & 0 & 0 \\ 0 & 0 & 0 & 1 \\ 0 & 0 & (\lambda + 2\mu) \partial_{x_2}^2 + \mu \partial_{x_1}^2 & 0 \end{pmatrix}$$

and

$$\mathbf{B} = \begin{pmatrix} 0 & 0 & 0 & 0 \\ 0 & 0 & (\lambda + \mu) \partial_{x_1} \partial_{x_2} & 0 \\ 0 & 0 & 0 & 0 \\ (\lambda + \mu) \partial_{x_1} \partial_{x_2} & 0 & 0 & 0 \end{pmatrix}.$$

This equation is integrated via *Strang’s splitting method* [44]. This splitting approach is known to be of order two and reads,

$$\exp((\mathbf{A} + \mathbf{B})t) = \exp(\mathbf{B}t/2) \exp(\mathbf{A}t) \exp(\mathbf{B}t/2) + o(t^2).$$

The operator  $\exp(\mathbf{A}t)$  is computed exactly in the spatial Fourier space. Indeed, the Fourier transform

$$\hat{P}_A(\xi, t) = \int P_A(x, t)e^{i\xi \cdot x} dx$$

of  $P_A(x, t) = \exp(\mathbf{A}t)P(x)$  is given explicitly by

$$\begin{cases} \widehat{u}_{A,1}(\xi, t) &= \cos\left(\sqrt{\xi_{\lambda,\mu,1}^2}t\right) \widehat{u}_1(\xi) + t \operatorname{sinc}\left(\sqrt{\xi_{\lambda,\mu,1}^2}t\right) \widehat{\partial}_t u_1(\xi), \\ \widehat{\partial}_t u_{A,1}(\xi, t) &= \cos\left(\sqrt{\xi_{\lambda,\mu,1}^2}t\right) \widehat{\partial}_t u_1(\xi) - \sqrt{\xi_{\lambda,\mu,1}^2} \operatorname{sinc}\left(\sqrt{\xi_{\lambda,\mu,1}^2}t\right) \widehat{u}_1(\xi), \\ \widehat{u}_{A,2}(\xi, t) &= \cos\left(\sqrt{\xi_{\lambda,\mu,2}^2}t\right) \widehat{u}_2(\xi) + t \operatorname{sinc}\left(\sqrt{\xi_{\lambda,\mu,2}^2}t\right) \widehat{\partial}_t u_2(\xi), \\ \widehat{\partial}_t u_{A,2}(\xi, t) &= \cos\left(\sqrt{\xi_{\lambda,\mu,2}^2}t\right) \widehat{\partial}_t u_2(\xi) - \sqrt{\xi_{\lambda,\mu,2}^2} \operatorname{sinc}\left(\sqrt{\xi_{\lambda,\mu,2}^2}t\right) \widehat{u}_2(\xi), \end{cases}$$

with

$$\xi_{\lambda,\mu,1}^2 = (\lambda + 2\mu)\xi_1^2 + \mu\xi_2^2, \quad \xi_{\lambda,\mu,2}^2 = (\lambda + 2\mu)\xi_2^2 + \mu\xi_1^2, \quad \text{and} \quad \operatorname{sinc}(t) = \sin(t)/t.$$

The second operator  $\exp(\mathbf{B}t)$  can also be integrated exactly, and the spatial Fourier transform of

$$P_B(x, t) = \exp(\mathbf{B}t)P(x)$$

is given explicitly by

$$\begin{cases} \widehat{u}_{B,1}(\xi, t) &= \widehat{u}_1(\xi), \\ \widehat{\partial}_t u_{B,1}(\xi, t) &= \widehat{\partial}_t u_1(\xi) + t\xi_{\lambda,\mu,3} \widehat{u}_2(\xi), \\ \widehat{u}_{B,2}(\xi, t) &= \widehat{u}_2(\xi), \\ \widehat{\partial}_t u_{B,2}(\xi, t) &= \widehat{\partial}_t u_2(\xi) + t\xi_{\lambda,\mu,3} \widehat{u}_1(\xi), \end{cases}$$

with

$$\xi_{\lambda,\mu,3} = (\lambda + \mu)\xi_1\xi_2.$$

This global algorithm appears to be stable under a classical condition of the form

$$\delta_t \leq c(\lambda, \mu)\delta_x^2,$$

where  $\delta_t$  and  $\delta_x$  denote, respectively, the time and the spatial step of discretization. Here  $c(\lambda, \mu)$  is a constant which depends only on the Lamé coefficients  $\lambda$  and  $\mu$ .

The functional  $\tilde{\mathcal{J}}(x)$  also requires a Helmholtz decomposition algorithm. As the support of the functional  $\tilde{\mathcal{J}}(x)$  is included in  $\Omega \subset Q$ , we use a homogeneous Neumann boundary condition on  $\partial Q$ . This decomposition is numerically obtained with a fast algorithm based on a symmetry principle and a Fourier–Helmholtz decomposition algorithm [50].



2.2.2 Experiments

In the sequel, for numerical illustrations,  $\Omega$  is taken as a unit disc. Its boundary is discretized by 1,024 sensors. Each solution of elastic wave equation is computed over  $(\mathbf{x}, t) \in [-L/2, L/2]^2 \times [0, T]$  with  $L = 4$  and  $T = 2$ . The discretization steps are  $dt = T/2^{13}$  and  $dx = L/2^9$ .

Figure 1 presents the first experiment with Lamé parameters  $(\lambda, \mu) = (1, 1)$ . The first (top) line corresponds to the two components of the initial source  $\mathbf{F}$ . The second line corresponds to the data  $\mathbf{g}(\mathbf{y}, t) = \mathbf{u}(\mathbf{y}, t)$  recorded over  $(\mathbf{y}, t) \in \partial\Omega \times [0, T]$ . Note that the shear and pressure waves are mixed in the recorded signal and it seems difficult to separate them. The third line corresponds to the imaging functional  $\mathcal{I}(\mathbf{x})$ . This example clearly shows that the reconstruction of the source  $\mathbf{F}$  is not so accurate with classical time-reversal imaging. Moreover, in the last row, the plots represent the modified imaging functional  $\tilde{\mathcal{I}}(\mathbf{x})$  where the reconstruction is clearly better.

Figure 2 shows another example with different Lamé parameters  $(\lambda, \mu) = (10, 1)$ . The same conclusion holds.

In Figure 3, we use a ‘less localized’ (large) source distribution. We observe some artifacts in the reconstruction of the imaging functional  $\tilde{\mathcal{I}}$ . We can also observe, from the recorded data, that the pressure and shear waves are very much *coupled* with each other. The artifacts in the reconstruction are the consequence of such coupling. In this situation, we do not have a normal incidence of the waves on  $\partial\Omega$ .

To conclude,  $\tilde{\mathcal{I}}$  provides a better reconstruction of the sources than  $\mathcal{I}$ . However, in certain cases, the reconstructions by  $\tilde{\mathcal{I}}$  are not optimal, and need further improvements. Several other challenging problems remain. It would be very interesting to extend the strategy developed in [3] to correct the effect of partial measurements in the elastic case. Another important problem is to correct the effect of random fluctuations in the elastic parameters. It is known that time-reversal techniques yield blurry images in such a case. Coherent interferometric techniques [14,15] may lead to better imaging in the elastic case as well.

3 Time-reversal algorithm for viscoelastic media

In this section we investigate the source inverse problem in an elastic attenuating medium. We provide an efficient regularized time-reversal imaging algorithm that corrects for the leading-order terms of the attenuation effect. Consider the viscoelastic wave equation in  $\mathbb{R}^d$  with  $d = 2, 3$ :

$$\begin{cases} \frac{\partial^2 \mathbf{u}_a}{\partial t^2}(\mathbf{x}, t) - \mathcal{L}_{\lambda, \mu} \mathbf{u}_a(\mathbf{x}, t) - \frac{\partial}{\partial t} \mathcal{L}_{\eta_\lambda, \eta_\mu} \mathbf{u}_a(\mathbf{x}, t) = \frac{d\delta_0(t)}{dt} \mathbf{F}(\mathbf{x}), & (\mathbf{x}, t) \in \mathbb{R}^d \times \mathbb{R}, \\ \mathbf{u}_a(\mathbf{x}, t) = \frac{\partial \mathbf{u}_a}{\partial t}(\mathbf{x}, t) = \mathbf{0}, & t < 0, \end{cases} \quad (3.1)$$

where the viscosity parameters  $\eta_\mu$  and  $\eta_\lambda$  are positive constants and account for losses in the medium. Let  $\mathbf{g}_a(\mathbf{x}, t) := \mathbf{u}_a(\mathbf{x}, t), \mathbf{x} \in \partial\Omega, t \in [0, T]$ . Again, the inverse problem is to reconstruct  $\mathbf{F}(\mathbf{x}), \mathbf{x} \in \Omega$  from  $\mathbf{g}_a(\mathbf{x}, t), \mathbf{x} \in \partial\Omega, t \in [0, T]$ . For solving the problem, we use a time-reversal approach.

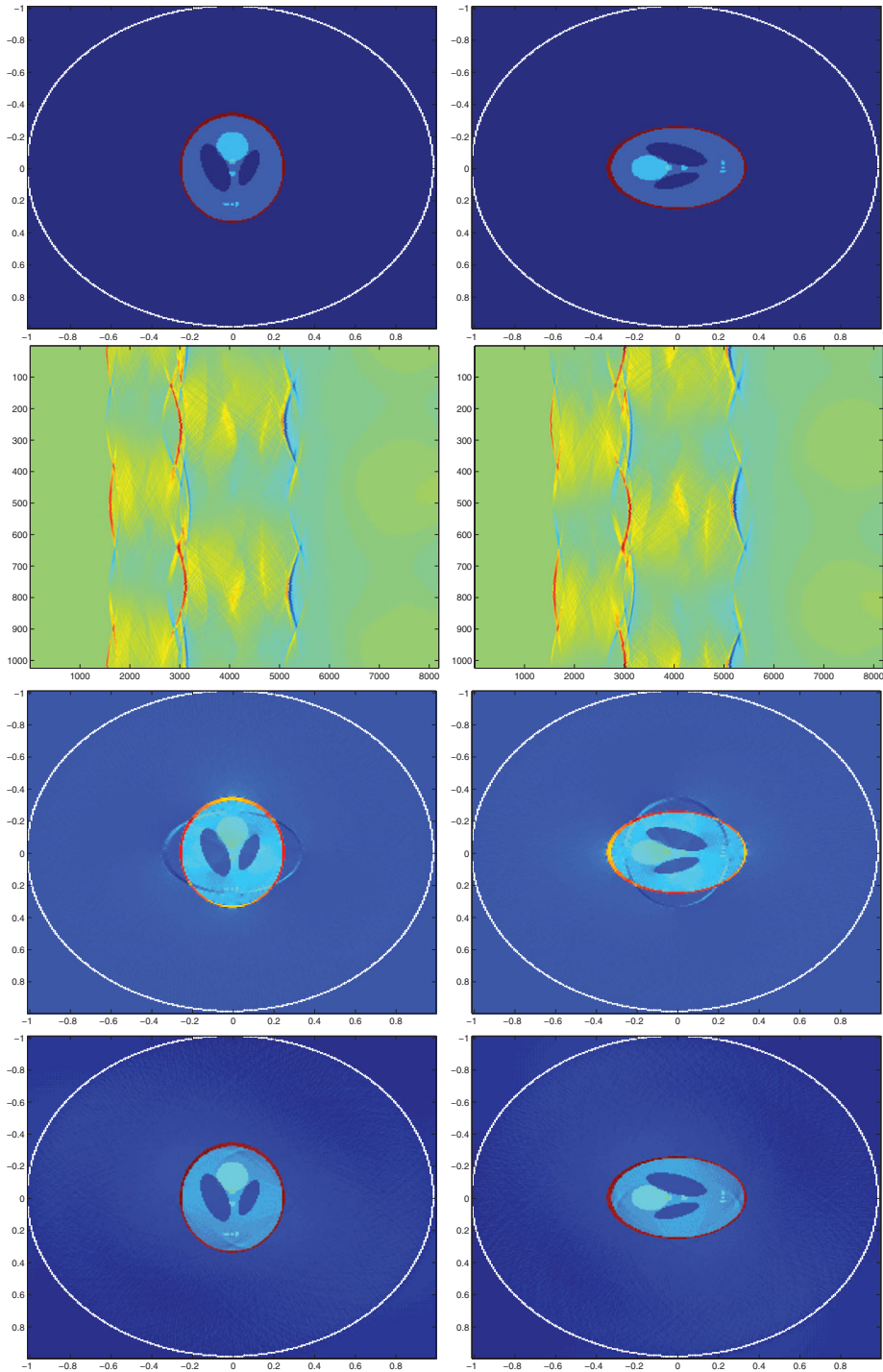


FIGURE 1. (Colour online) Source reconstruction. Comparison between the imaging functionals  $\mathcal{I}$  and  $\tilde{\mathcal{I}}$  with Lamé constants  $(\lambda, \mu) = (1, 1)$ . From top to bottom: First line: the source  $\mathbf{F}$ ; second line: recorded data  $g(\mathbf{y}, t)$ ; third line: imaging functional  $\mathcal{I}$ ; last line: imaging functional  $\tilde{\mathcal{I}}$ .

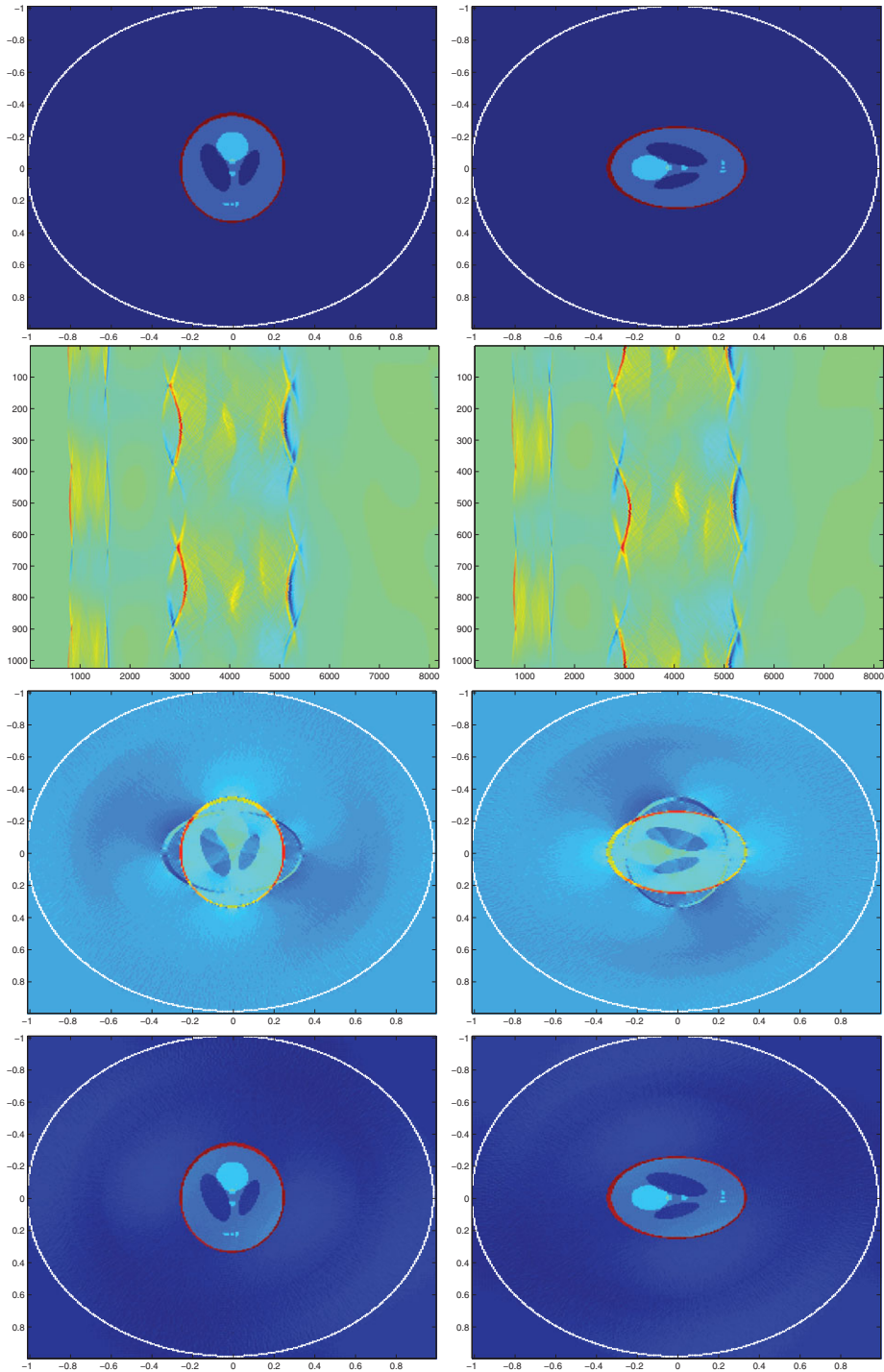


FIGURE 2. (Colour online) Source reconstruction. Comparison between the imaging functionals  $\mathcal{I}$  and  $\tilde{\mathcal{I}}$  with Lamé constants  $(\lambda, \mu) = (10, 1)$ . First line: source  $F$ ; second line: recorded data  $g(y, t)$ ; third line: imaging functional  $\mathcal{I}$ ; last line: imaging functional  $\tilde{\mathcal{I}}$ .

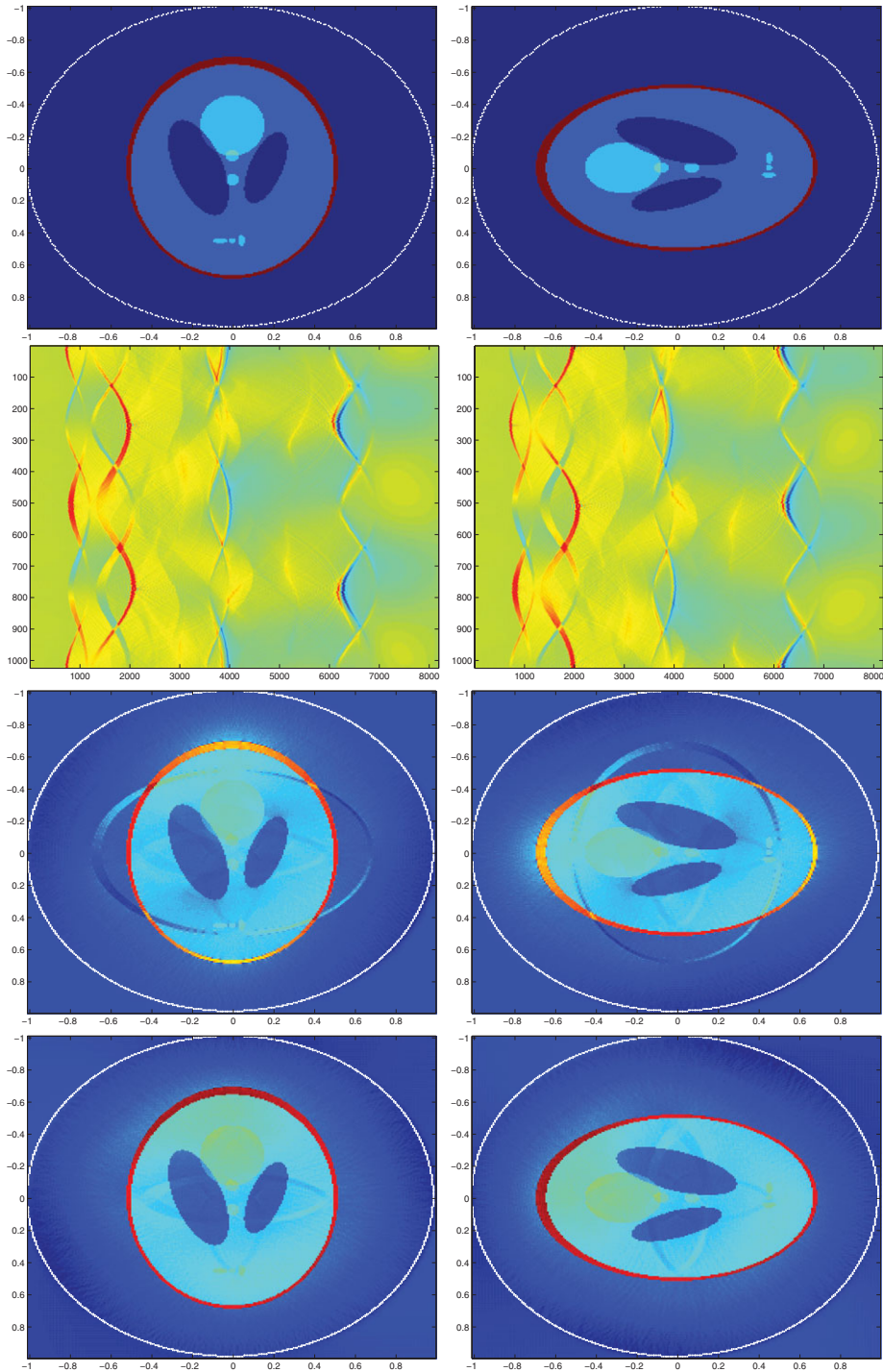


FIGURE 3. (Colour online) Source reconstruction. Comparison between the imaging functionals  $\mathcal{I}$  and  $\tilde{\mathcal{I}}$  with Lamé constants  $(\lambda, \mu) = (1, 1)$  and less localized source than in Figure 1. First line: source  $F$ ; second line: recorded data  $g(y, t)$ ; third line: imaging functional  $\mathcal{I}$ ; last line: imaging functional  $\tilde{\mathcal{I}}$ .

Before doing so, it is worth mentioning that there are several other models for attenuation. Empirically, attenuation in viscoelastic media obeys a frequency power law-type attenuation, whereas thermo-viscous model considered here is a special case. In this regard, we refer to [17, 38, 45 and references therein]. As the present work is motivated by biomedical imaging techniques, and the thermo-viscous model (also known as the Kelvin–Voigt model) is well justified in modelling viscoelastic behaviour of a large class of elastic materials, including soft tissues [20], we therefore concentrate on thermo-viscous model. In the acoustic case in [5, 7], the acoustic counterpart of the present inverse problem where generalized type of power-law attenuation is dealt with. The analysis therein is presented first for thermo-viscous model and then a simple procedure is devised to extend the analysis therein to general power-law models using an argument of fractional Laplacian and dominated convergence theorem of Lebesgue. Here a very similar remark holds, since a viscoelastic wave can be converted to two acoustic-type waves using Helmholtz decompositions, and the results presented in this paper can be extended easily to general viscoelastic models. For acoustic power-law attenuation models and reconstruction algorithms, see [33].

We now turn to time reversal in viscoelastic media. As in the acoustic case [5], the strategy of time reversal is to consider the functional

$$\mathcal{J}_a(\mathbf{x}) = \int_0^T v_{s,a}(\mathbf{x}, T) ds, \tag{3.2}$$

where  $v_{s,a}$  should be the *solution* of the adjoint (time-reversed) viscoelastic wave equation, i.e.

$$\begin{cases} \frac{\partial^2 v_{s,a}}{\partial t^2}(\mathbf{x}, t) - \mathcal{L}_{\lambda,\mu} v_{s,a}(\mathbf{x}, t) \\ \quad + \frac{\partial}{\partial t} \mathcal{L}_{\eta,\nu} v_{s,a}(\mathbf{x}, t) = \frac{d\delta_s(t)}{dt} g_a(\mathbf{x}, T - s) \delta_{\partial\Omega}(\mathbf{x}), & (\mathbf{x}, t) \in \mathbb{R}^d \times \mathbb{R}, \\ v_{s,a}(\mathbf{x}, t) = \frac{\partial v_{s,a}}{\partial t}(\mathbf{x}, t) = \mathbf{0} & \mathbf{x} \in \mathbb{R}^d, t < s. \end{cases} \tag{3.3}$$

Further, the idea is to enhance image resolution using  $\tilde{\mathcal{J}}_a$ , as in purely elastic media, where

$$\tilde{\mathcal{J}}_a = c_S \mathcal{H}^S [\mathcal{J}_a] + c_P \mathcal{H}^P [\mathcal{J}_a].$$

Unfortunately, the adjoint viscoelastic problem is severely ill-posed. Indeed, the high-frequency components are exponentially increasing due to the presence of the *anti-damping* term

$$\left( +\partial_t \mathcal{L}_{\eta,\nu} v_{s,a} \right),$$

which induces instability. Therefore, we need to regularize the adjoint problem by truncating high-frequency components either in time or in space.

For  $\mathbf{y} \in \mathbb{R}^d$  let us introduce the time-dependent Green tensor  $\mathbf{G}_a$  associated to the viscoelastic wave equation which is the solution to

$$\begin{cases} \frac{\partial^2 \mathbf{G}_a}{\partial t^2}(\mathbf{x}, \mathbf{y}, t) - \mathcal{L}_{\lambda, \mu} \mathbf{G}_a(\mathbf{x}, \mathbf{y}, t) - \frac{\partial}{\partial t} \mathcal{L}_{\eta_\lambda, \eta_\mu} \mathbf{G}_a(\mathbf{x}, \mathbf{y}, t) = \frac{d\delta_0(t)}{dt} \delta_{\mathbf{y}}(\mathbf{x}), & (\mathbf{x}, t) \in \mathbb{R}^d \times \mathbb{R}, \\ \mathbf{G}_a(\mathbf{x}, \mathbf{y}, t) = \frac{\partial \mathbf{G}_a}{\partial t}(\mathbf{x}, \mathbf{y}, t) = \mathbf{0}, & t < 0. \end{cases} \tag{3.4}$$

We denote by  $\hat{\mathbf{G}}_{a, \omega}$  its temporal Fourier transform. It is the outgoing time-harmonic Green tensor solution of

$$(\mathcal{L}_{\lambda, \mu} - i\omega \mathcal{L}_{\eta_\lambda, \eta_\mu} + \omega^2) \hat{\mathbf{G}}_{a, \omega}(\mathbf{x}, \mathbf{y}) = -\delta_{\mathbf{y}}(\mathbf{x}) \mathbf{I}, \quad \mathbf{x}, \mathbf{y} \in \mathbb{R}^d. \tag{3.5}$$

We also introduce the *adjoint* viscoelastic Green tensor  $\hat{\mathbf{G}}_{-a, \omega}$ . It is the solution to

$$(\mathcal{L}_{\lambda, \mu} + i\omega \mathcal{L}_{\eta_\lambda, \eta_\mu} + \omega^2) \hat{\mathbf{G}}_{-a, \omega}(\mathbf{x}, \mathbf{y}) = -\delta_{\mathbf{y}}(\mathbf{x}) \mathbf{I}, \quad \mathbf{x}, \mathbf{y} \in \mathbb{R}^d. \tag{3.6}$$

We introduce an approximation  $\mathbf{v}_{s, a, \rho}$  of the adjoint wave  $\mathbf{v}_{s, a}$  by

$$\mathbf{v}_{s, a, \rho}(\mathbf{x}, t) = -\frac{1}{2\pi} \int_{|\omega| \leq \rho} \left\{ \int_{\partial\Omega} i\omega \hat{\mathbf{G}}_{-a, \omega}(\mathbf{x}, \mathbf{y}) \mathbf{g}_a(\mathbf{y}, T - s) d\sigma(\mathbf{y}) \right\} \exp(-i\omega(t - s)) d\omega, \tag{3.7}$$

where  $\rho \in \mathbb{R}^+$  is the cut-off parameter. The regularized time-reversal imaging functional defined by

$$\mathcal{I}_{a, \rho}(\mathbf{x}) = \int_0^T \mathbf{v}_{s, a, \rho}(\mathbf{x}, T) ds \tag{3.8}$$

can be written as

$$\mathcal{I}_{a, \rho}(\mathbf{x}) = - \int_{\partial\Omega} \int_0^T \frac{\partial}{\partial s} \left[ \mathbf{G}_{-a, \rho}(\mathbf{x}, \mathbf{y}, T - s) \right] \mathbf{g}_a(\mathbf{y}, T - s) ds d\sigma(\mathbf{y}), \tag{3.9}$$

where

$$\mathbf{G}_{-a, \rho}(\mathbf{x}, \mathbf{y}, t) = \frac{1}{2\pi} \int_{|\omega| \leq \rho} \hat{\mathbf{G}}_{-a, \omega}(\mathbf{x}, \mathbf{y}) \exp(-i\omega t) d\omega. \tag{3.10}$$

**Remark 3.1** Let  $\mathcal{S}'$  be the space of tempered distributions, *i.e.* the dual of the Schwartz space  $\mathcal{S}$  of rapidly decreasing functions [32]. The function  $\mathbf{v}_{s, a, \rho}(\mathbf{x}, t)$  can be identified as the solution of the following wave equation:

$$\frac{\partial^2 \mathbf{v}_{s, a, \rho}}{\partial t^2}(\mathbf{x}, t) - \mathcal{L}_{\lambda, \mu} \mathbf{v}_{s, a, \rho}(\mathbf{x}, t) + \frac{\partial}{\partial t} \mathcal{L}_{\eta_\lambda, \eta_\mu} \mathbf{v}_{s, a, \rho}(\mathbf{x}, t) = S_\rho \left[ \frac{d\delta_s(t)}{dt} \right] \mathbf{g}_a(\mathbf{x}, T - s) \delta_{\partial\Omega}(\mathbf{x}), \tag{3.11}$$

where the operator  $S_\rho$  is defined on the space  $\mathcal{S}'$  by

$$S_\rho [\psi](t) = \frac{1}{2\pi} \int_{|\omega| \leq \rho} \exp(-i\omega t) \hat{\psi}(\omega) d\omega, \tag{3.12}$$

with

$$\hat{\psi}(\omega) = \int_{\mathbb{R}} \psi(t) \exp(i\omega t) dt. \tag{3.13}$$

### 3.1 Green’s tensor in viscoelastic media

As in Section 2, we decompose  $\hat{\mathbf{G}}_{\pm a, \omega}$  in the form

$$\hat{\mathbf{G}}_{\pm a, \omega} = \hat{\mathbf{G}}_{\pm a, \omega}^S + \hat{\mathbf{G}}_{\pm a, \omega}^P, \tag{3.14}$$

where  $\hat{\mathbf{G}}_{\pm a, \omega}^S$  and  $\hat{\mathbf{G}}_{\pm a, \omega}^P$  are, respectively, the fundamental solutions of

$$(\mathcal{L}_{\lambda, \mu} \mp i\omega \mathcal{L}_{\eta_\lambda, \eta_\mu} + \omega^2) \hat{\mathbf{G}}_{\pm a, \omega}^\alpha(\mathbf{x}, \mathbf{y}) = \mathcal{H}^\alpha [-\delta_{\mathbf{y}} \mathbf{I}](\mathbf{x}), \quad \alpha = P, S. \tag{3.15}$$

Let us also introduce the decomposition of the operator  $\mathcal{L}_{\lambda, \mu}$  into shear and pressure components as

$$\mathcal{L}_{\lambda, \mu} = \mathcal{L}_{\lambda, \mu}^S + \mathcal{L}_{\lambda, \mu}^P, \quad \text{and} \quad \mathcal{L}_{\eta_\lambda, \eta_\mu} = \mathcal{L}_{\eta_\lambda, \eta_\mu}^S + \mathcal{L}_{\eta_\lambda, \eta_\mu}^P, \tag{3.16}$$

where

$$\mathcal{L}_{\lambda, \mu}^S \mathbf{u} = c_S^2 [\Delta \mathbf{u} - \nabla(\nabla \cdot \mathbf{u})] \quad \text{and} \quad \mathcal{L}_{\lambda, \mu}^P \mathbf{u} = c_P^2 \nabla(\nabla \cdot \mathbf{u}), \tag{3.17}$$

and

$$\mathcal{L}_{\eta_\lambda, \eta_\mu}^S \mathbf{u} = c_S^2 \varepsilon_S [\Delta \mathbf{u} - \nabla(\nabla \cdot \mathbf{u})] \quad \text{and} \quad \mathcal{L}_{\eta_\lambda, \eta_\mu}^P \mathbf{u} = c_P^2 \varepsilon_P \nabla(\nabla \cdot \mathbf{u}). \tag{3.18}$$

Here we have defined

$$\varepsilon_S = \frac{\eta_\mu}{\mu} \quad \text{and} \quad \varepsilon_P = \frac{\eta_\lambda + 2\eta_\mu}{\lambda + 2\mu}. \tag{3.19}$$

Therefore, the tensors  $\hat{\mathbf{G}}_{\pm a, \omega}^S$  and  $\hat{\mathbf{G}}_{\pm a, \omega}^P$  are also solutions of

$$(\mathcal{L}_{\lambda, \mu}^\alpha \mp i\omega \mathcal{L}_{\eta_\lambda, \eta_\mu}^\alpha + \omega^2) \hat{\mathbf{G}}_{\pm a, \omega}^\alpha(\mathbf{x}, \mathbf{y}) = \mathcal{H}^\alpha [-\delta_{\mathbf{y}} \mathbf{I}](\mathbf{x}), \quad \alpha = P, S. \tag{3.20}$$

The corrected regularized time-reversal imaging functional defined by

$$\tilde{\mathcal{I}}_{a, \rho} = c_S \mathcal{H}^S [\mathcal{I}_{a, \rho}] + c_P \mathcal{H}^P [\mathcal{I}_{a, \rho}] \tag{3.21}$$

is then given by

$$\tilde{\mathcal{I}}_{a, \rho}(\mathbf{x}) = - \int_{\partial\Omega} \int_0^T \frac{\partial}{\partial s} [c_P \mathbf{G}_{-a, \rho}^P(\mathbf{x}, \mathbf{y}, T-s) + c_S \mathbf{G}_{-a, \rho}^S(\mathbf{x}, \mathbf{y}, T-s)] \mathbf{g}_a(\mathbf{y}, T-s) ds d\sigma(\mathbf{y}), \tag{3.22}$$

where

$$\mathbf{G}_{-a, \rho}^\alpha(\mathbf{x}, \mathbf{y}, t) = \frac{1}{2\pi} \int_{|\omega| \leq \rho} \hat{\mathbf{G}}_{-a, \omega}^\alpha(\mathbf{x}, \mathbf{y}) \exp(-i\omega t) d\omega, \quad \alpha = P, S. \tag{3.23}$$

In the next section we express the relationship between the data  $\mathbf{g}_a$  and the ideal measurements  $\mathbf{g}$  obtained in the non-attenuated case. By doing so we prove with the help of a new version of the Helmholtz–Kirchhoff identity that a regularized image of the source  $\mathbf{F}$  can be obtained.

**3.2 Attenuation operator and its asymptotics**

Recall that  $\mathbf{u}$  and  $\mathbf{u}_a$  are, respectively, the solutions of the wave equations

$$\frac{\partial^2 \mathbf{u}}{\partial t^2}(\mathbf{x}, t) - \mathcal{L}_{\lambda, \mu} \mathbf{u}(\mathbf{x}, t) = \frac{d\delta_0(t)}{dt} \mathbf{F}(\mathbf{x}), \tag{3.24}$$

and

$$\frac{\partial^2 \mathbf{u}_a}{\partial t^2}(\mathbf{x}, t) - \mathcal{L}_{\lambda, \mu} \mathbf{u}_a(\mathbf{x}, t) - \frac{\partial}{\partial t} \mathcal{L}_{\eta_\lambda, \eta_\mu} \mathbf{u}_a(\mathbf{x}, t) = \frac{d\delta_0(t)}{dt} \mathbf{F}(\mathbf{x}), \tag{3.25}$$

with the initial conditions

$$\mathbf{u}(\mathbf{x}, t) = \mathbf{u}_a(\mathbf{x}, t) = \frac{\partial \mathbf{u}}{\partial t}(\mathbf{x}, t) = \frac{\partial \mathbf{u}_a}{\partial t}(\mathbf{x}, t) = \mathbf{0}, \quad t < 0. \tag{3.26}$$

We decompose  $\mathbf{u}$  and  $\mathbf{u}_a$  as

$$\mathbf{u} = \mathbf{u}^S + \mathbf{u}^P = \mathcal{H}^S[\mathbf{u}] + \mathcal{H}^P[\mathbf{u}] \quad \text{and} \quad \mathbf{u}_a = \mathbf{u}_a^S + \mathbf{u}_a^P = \mathcal{H}^S[\mathbf{u}_a] + \mathcal{H}^P[\mathbf{u}_a]. \tag{3.27}$$

The temporal Fourier transforms  $\hat{\mathbf{u}}_\omega^\alpha$  and  $\hat{\mathbf{u}}_{a,\omega}^\alpha$  of the vector functions  $\mathbf{u}^\alpha$  and  $\mathbf{u}_a^\alpha$  are, respectively, solutions of

$$(\omega^2 + \mathcal{L}_{\lambda, \mu}^\alpha) \hat{\mathbf{u}}_\omega^\alpha = i\omega \mathcal{H}^\alpha[\mathbf{F}] \quad \text{and} \quad (\kappa_{\varepsilon_\alpha}(\omega)^2 + \mathcal{L}_{\lambda, \mu}^\alpha) \hat{\mathbf{u}}_{a,\omega}^\alpha = i \frac{\kappa_{\varepsilon_\alpha}(\omega)^2}{\omega} \mathcal{H}^\alpha[\mathbf{F}], \quad \alpha = P, S, \tag{3.28}$$

where

$$\kappa_\varepsilon(\omega) = \frac{\omega}{\sqrt{1 - i\omega\varepsilon}}. \tag{3.29}$$

In particular, it implies that

$$\mathbf{u}_a^S = \mathcal{A}_{\varepsilon_S}[\mathbf{u}^S] \quad \text{and} \quad \mathbf{u}_a^P = \mathcal{A}_{\varepsilon_P}[\mathbf{u}^P], \tag{3.30}$$

where  $\mathcal{A}_\varepsilon$ , for  $\varepsilon > 0$ , is the attenuation operator

$$\mathcal{A}_\varepsilon[\phi](t) = \frac{1}{2\pi} \int_{\mathbb{R}} \frac{\kappa_\varepsilon(\omega)}{\omega} \left\{ \int_{\mathbb{R}^+} \phi(s) \exp\{i\kappa_\varepsilon(\omega)s\} ds \right\} \exp\{-i\omega t\} d\omega, \quad t > 0. \tag{3.31}$$

We also define the operator  $\mathcal{A}_{-\varepsilon, \rho}$  by

$$\mathcal{A}_{-\varepsilon, \rho}[\phi](t) = \frac{1}{2\pi} \int_{\mathbb{R}^+} \phi(s) \left\{ \int_{|\omega| \leq \rho} \frac{\kappa_{-\varepsilon}(\omega)}{\omega} \exp\{i\kappa_{-\varepsilon}(\omega)s\} \exp\{-i\omega t\} d\omega \right\} ds, \tag{3.32}$$

which is associated with  $\kappa_{-\varepsilon}(\omega) = \frac{\omega}{\sqrt{1 + i\omega\varepsilon}}$ . Moreover, its adjoint operator  $\mathcal{A}_{-\varepsilon, \rho}^*$  reads

$$\mathcal{A}_{-\varepsilon, \rho}^*[\phi](t) = \frac{1}{2\pi} \int_{|\omega| \leq \rho} \frac{\kappa_{-\varepsilon}(\omega)}{\omega} \exp\{i\kappa_{-\varepsilon}(\omega)t\} \left\{ \int_{\mathbb{R}^+} \phi(s) \exp\{-i\omega s\} ds \right\} d\omega. \tag{3.33}$$

We extend the operators  $\mathcal{A}_\varepsilon$ ,  $\mathcal{A}_{-\varepsilon, \rho}$  and  $\mathcal{A}_{-\varepsilon, \rho}^*$  to tensors  $\mathbf{G}$ , i.e. for all vectors  $\mathbf{p} \in \mathbb{R}^d$ ,

$$\mathcal{A}_\varepsilon[\mathbf{G}\mathbf{p}] = \mathcal{A}_\varepsilon[\mathbf{G}]\mathbf{p}, \quad \mathcal{A}_{-\varepsilon, \rho}[\mathbf{G}\mathbf{p}] = \mathcal{A}_{-\varepsilon, \rho}[\mathbf{G}]\mathbf{p} \quad \text{and} \quad \mathcal{A}_{-\varepsilon, \rho}^*[\mathbf{G}\mathbf{p}] = \mathcal{A}_{-\varepsilon, \rho}^*[\mathbf{G}]\mathbf{p}.$$



By the definition of the operators  $\mathcal{A}_\varepsilon$  and  $\mathcal{A}_{-\varepsilon,\rho}$ , we have for  $\alpha = P, S$ :

$$\frac{\partial \mathbf{G}_a^\alpha}{\partial t}(\mathbf{x}, \mathbf{y}, t) = \mathcal{A}_{\varepsilon_x} \left[ \frac{\partial \mathbf{G}^\alpha}{\partial t}(\mathbf{x}, \mathbf{y}, \cdot) \right] (t), \tag{3.34}$$

$$\frac{\partial \mathbf{G}_{-a,\rho}^\alpha}{\partial t}(\mathbf{x}, \mathbf{y}, t) = \mathcal{A}_{-\varepsilon_x,\rho} \left[ \frac{\partial \mathbf{G}^\alpha}{\partial t}(\mathbf{x}, \mathbf{y}, \cdot) \right] (t). \tag{3.35}$$

It is worth emphasizing that identities (3.34) and (3.35) are exact. They are particular cases of (3.30) with  $\mathbf{F}(\mathbf{x}) = \delta_{\mathbf{y}}(\mathbf{x})\mathbf{I}$ . They still hold for other attenuation models as shown in [33].

We need the following results from [5, 7].

**Proposition 3.2**

- Let  $\phi(t) \in \mathcal{S}([0, \infty))$ ,  $\mathcal{S}$  being the Schwartz space. Then

$$\mathcal{A}_\varepsilon[\phi](t) = \phi(t) + \frac{\varepsilon}{2} (t\phi')'(t) + o(\varepsilon) \quad \text{as } \varepsilon \rightarrow 0. \tag{3.36}$$

- Let  $\phi(t) \in \mathcal{D}([0, \infty))$ , where  $\mathcal{D}([0, \infty))$  is the space of  $\mathcal{C}^\infty$ -functions of compact support on  $[0, \infty)$ . Then, for all  $\rho > 0$ ,

$$\mathcal{A}_{-\varepsilon,\rho}^*[\phi](t) = S_\rho[\phi](t) - \frac{\varepsilon}{2} S_\rho[(t\phi')'](t) + o(\varepsilon) \quad \text{as } \varepsilon \rightarrow 0, \tag{3.37}$$

where  $S_\rho$  is defined by (3.12).

- Let  $\phi(t) \in \mathcal{D}([0, \infty))$ . Then, for all  $\rho > 0$ ,

$$\mathcal{A}_{-\varepsilon,\rho}^* \mathcal{A}_\varepsilon[\phi](t) = S_\rho[\phi](t) + o(\varepsilon) \quad \text{as } \varepsilon \rightarrow 0. \tag{3.38}$$

Recall that  $\mathbf{g} = \mathbf{u}$  and  $\mathbf{g}_a = \mathbf{u}_a$  on  $\partial\Omega \times [0, T]$ . It then follows from (3.30) that, for  $\alpha = P, S$ , and  $\varepsilon_x \rightarrow 0$ ,

$$\mathcal{A}_{-\varepsilon_x,\rho}^* \mathcal{A}_{\varepsilon_x}[\mathbf{g}_a^\alpha] = S_\rho[\mathbf{g}^\alpha] + o(\varepsilon_x), \tag{3.39}$$

where

$$\mathbf{g}_a^\alpha = \mathcal{H}^\alpha[\mathbf{g}_a], \quad \mathbf{g}^\alpha = \mathcal{H}^\alpha[\mathbf{g}]. \tag{3.40}$$

Identity (3.39) proves that  $\mathcal{A}_{-\varepsilon_x,\rho}^*$  is an approximate inverse of  $\mathcal{A}_{\varepsilon_x}$ . Moreover, it plays a key role in showing that the regularized time-reversal algorithm provides a first-order correction of the attenuation effect.

### 3.3 Helmholtz–Kirchhoff identity in attenuating media

In this section we derive a new Helmholtz–Kirchhoff identity in elastic attenuating media. For doing so, let us introduce the conormal derivatives  $\partial \mathbf{u} / \partial v_a$  and  $\partial \mathbf{u} / \partial v_{-a}$  as follows:

$$\frac{\partial \mathbf{u}}{\partial v_{\pm a}} := (\lambda(\nabla \cdot \mathbf{u})\mathbf{n} + \mu(\nabla \mathbf{u}^T + (\nabla \mathbf{u}^T)^T)\mathbf{n}) \mp i\omega (\eta_\lambda(\nabla \cdot \mathbf{u})\mathbf{n} + \eta_\mu(\nabla \mathbf{u}^T + (\nabla \mathbf{u}^T)^T)\mathbf{n}). \tag{3.41}$$

Note also that for a tensor  $\mathbf{G}$  the conormal derivative  $\frac{\partial \mathbf{G}}{\partial v_{\pm a}}$  means that for all constant vectors  $\mathbf{p}$ ,

$$\left[ \frac{\partial \mathbf{G}}{\partial v_{\pm a}} \right] \mathbf{p} := \frac{\partial [\mathbf{G}\mathbf{p}]}{\partial v_{\pm a}}. \tag{3.42}$$

The following properties hold.

**Proposition 3.3** *For all  $\mathbf{x}, \mathbf{z} \in \Omega$ , we have*

$$\int_{\partial\Omega} \left[ \frac{\partial \hat{\mathbf{G}}_{-a,\omega}^S(\mathbf{x}, \mathbf{y})}{\partial v_{-a}} \overline{\hat{\mathbf{G}}_{a,\omega}^P(\mathbf{y}, \mathbf{z})} - \hat{\mathbf{G}}_{-a,\omega}^S(\mathbf{x}, \mathbf{y}) \frac{\partial \overline{\hat{\mathbf{G}}_{a,\omega}^P(\mathbf{y}, \mathbf{z})}}{\partial v_a} \right] d\sigma(\mathbf{y}) = 0. \tag{3.43}$$

**Proof** For  $\mathbf{x}, \mathbf{z} \in \Omega$ ,

$$\begin{aligned} \mathcal{J}(\mathbf{x}, \mathbf{z}) &:= \int_{\partial\Omega} \left[ \frac{\partial \hat{\mathbf{G}}_{-a,\omega}^S(\mathbf{x}, \mathbf{y})}{\partial v_{-a}} \overline{\hat{\mathbf{G}}_{a,\omega}^P(\mathbf{y}, \mathbf{z})} - \hat{\mathbf{G}}_{-a,\omega}^S(\mathbf{x}, \mathbf{y}) \frac{\partial \overline{\hat{\mathbf{G}}_{a,\omega}^P(\mathbf{y}, \mathbf{z})}}{\partial v_a} \right] d\sigma(\mathbf{y}) \\ &= \int_{\partial\Omega} \left[ \frac{\partial \hat{\mathbf{G}}_{-a,\omega}^S(\mathbf{x}, \mathbf{y})}{\partial v_{-a}} \overline{\hat{\mathbf{G}}_{a,\omega}^P(\mathbf{y}, \mathbf{z})} - \hat{\mathbf{G}}_{-a,\omega}^S(\mathbf{x}, \mathbf{y}) \frac{\partial \overline{\hat{\mathbf{G}}_{a,\omega}^P(\mathbf{y}, \mathbf{z})}}{\partial v_{-a}} \right] d\sigma(\mathbf{y}) \\ &= \int_{\Omega} \left[ \mathcal{L}_{\lambda,\mu} \hat{\mathbf{G}}_{-a,\omega}^S(\mathbf{x}, \mathbf{y}) + i\omega \mathcal{L}_{\eta_\lambda, \eta_\mu} \hat{\mathbf{G}}_{-a,\omega}^S(\mathbf{x}, \mathbf{y}) \right] \overline{\hat{\mathbf{G}}_{a,\omega}^P(\mathbf{y}, \mathbf{z})} d\mathbf{y} \\ &\quad - \int_{\Omega} \hat{\mathbf{G}}_{-a,\omega}^S(\mathbf{x}, \mathbf{y}) \left[ \mathcal{L}_{\lambda,\mu} \overline{\hat{\mathbf{G}}_{a,\omega}^P(\mathbf{y}, \mathbf{z})} + i\omega \mathcal{L}_{\eta_\lambda, \eta_\mu} \overline{\hat{\mathbf{G}}_{a,\omega}^P(\mathbf{y}, \mathbf{z})} \right] d\mathbf{y}, \\ &= \int_{\Omega} \left[ \mathcal{L}_{\lambda,\mu} \hat{\mathbf{G}}_{-a,\omega}^S(\mathbf{x}, \mathbf{y}) + i\omega \mathcal{L}_{\eta_\lambda, \eta_\mu} \hat{\mathbf{G}}_{-a,\omega}^S(\mathbf{x}, \mathbf{y}) \right] \overline{\hat{\mathbf{G}}_{a,\omega}^P(\mathbf{y}, \mathbf{z})} d\mathbf{y} \\ &\quad - \int_{\Omega} \hat{\mathbf{G}}_{-a,\omega}^S(\mathbf{x}, \mathbf{y}) \overline{\left[ \mathcal{L}_{\lambda,\mu} \hat{\mathbf{G}}_{a,\omega}^P(\mathbf{y}, \mathbf{z}) - i\omega \mathcal{L}_{\eta_\lambda, \eta_\mu} \hat{\mathbf{G}}_{a,\omega}^P(\mathbf{y}, \mathbf{z}) \right]} d\mathbf{y}. \end{aligned}$$

Since  $\hat{\mathbf{G}}_{a,\omega}^P(\mathbf{x}, \mathbf{y})$  and  $\hat{\mathbf{G}}_{-a,\omega}^S(\mathbf{x}, \mathbf{y})$  are solutions of (3.15) with  $\alpha = P, S$ , respectively, it follows that

$$\mathcal{J}(\mathbf{x}, \mathbf{z}) = [\mathcal{H}^S[-\delta_0 \mathbf{I}] * \overline{\hat{\mathbf{G}}_{a,\omega}^P(\cdot, \mathbf{z})}](\mathbf{x}) - [\hat{\mathbf{G}}_{-a,\omega}^S(\mathbf{x}, \cdot) * \mathcal{H}^P[-\delta_0 \mathbf{I}]](\mathbf{z}).$$

As in the proof of Proposition 2.2, one can show that

$$[\mathcal{H}^S[-\delta_0 \mathbf{I}] * \overline{\hat{\mathbf{G}}_{a,\omega}^P(\cdot, \mathbf{z})}](\mathbf{x}) = 0 \quad \text{and} \quad [\hat{\mathbf{G}}_{-a,\omega}^S(\mathbf{x}, \cdot) * \mathcal{H}^P[-\delta_0 \mathbf{I}]](\mathbf{z}) = 0,$$

which completes the proof of the proposition. □

We now give an approximation of the viscoelastic conormal derivative, which holds only for homogeneous isotropic elastic media.

**Proposition 3.4** *If  $\mathbf{n} = \widehat{\mathbf{y} - \mathbf{x}}$ , then for  $\alpha = P, S$ , we have*

$$\frac{\partial \hat{\mathbf{G}}_{\pm a, \omega}^{\alpha}(\mathbf{x}, \mathbf{y})}{\partial v_{\pm a}} \simeq \frac{ic_{\alpha} \omega^2}{\kappa_{\pm \varepsilon_{\alpha}}(\omega)} \hat{\mathbf{G}}_{\pm a, \omega}^{\alpha}(\mathbf{x}, \mathbf{y}), \quad (3.44)$$

where

$$\kappa_{\pm \varepsilon}(\omega) = \frac{\omega}{\sqrt{1 \mp i\omega\varepsilon}}. \quad (3.45)$$

**Proof** Indeed, note that (see Appendix)

$$\hat{\mathbf{G}}_{\pm a, \omega}^{\alpha}(\mathbf{x}, \mathbf{y}) = \left[ \frac{\kappa_{\pm \varepsilon_{\alpha}}(\omega)}{\omega} \right]^2 \hat{\mathbf{G}}_{\kappa_{\pm \varepsilon_{\alpha}}(\omega)}^{\alpha}(\mathbf{x}, \mathbf{y}), \quad \alpha = P, S. \quad (3.46)$$

Then, from Proposition 2.4, we obtain

$$\begin{aligned} & \frac{\partial \hat{\mathbf{G}}_{\pm a, \omega}^{\alpha}(\mathbf{x}, \mathbf{y})}{\partial v_{\pm a}} \\ & \simeq \left[ \frac{\kappa_{\pm \varepsilon_{\alpha}}(\omega)}{\omega} \right]^2 \left( \left( ic_{\alpha}^2 \frac{\kappa_{\pm \varepsilon_{\alpha}}(\omega)}{c_{\alpha}} \hat{\mathbf{G}}_{\kappa_{\pm \varepsilon_{\alpha}}(\omega)}^{\alpha}(\mathbf{x}, \mathbf{y}) \right) \mp i\omega \left( ic_{\alpha}^2 \varepsilon_{\alpha} \frac{\kappa_{\pm \varepsilon_{\alpha}}(\omega)}{c_{\alpha}} \hat{\mathbf{G}}_{\kappa_{\pm \varepsilon_{\alpha}}(\omega)}^{\alpha}(\mathbf{x}, \mathbf{y}) \right) \right) \\ & \simeq [ic_{\alpha} \kappa_{\pm \varepsilon_{\alpha}}(\omega) (1 \mp i\omega\varepsilon_{\alpha})] \hat{\mathbf{G}}_{\pm a, \omega}^{\alpha}(\mathbf{x}, \mathbf{y}) \simeq \frac{ic_{\alpha} \omega^2}{\kappa_{\pm \varepsilon_{\alpha}}(\omega)} \hat{\mathbf{G}}_{\pm a, \omega}^{\alpha}(\mathbf{x}, \mathbf{y}), \end{aligned}$$

which completes the proof.  $\square$

In particular, the following estimate holds as a direct consequence of Propositions 3.3 and 3.4.

**Proposition 3.5** *Let  $\Omega \subset \mathbb{R}^d$  be a ball with large radius  $R$ . Then for all  $\mathbf{x}, \mathbf{z} \in \Omega$  sufficiently far (with respect to wavelengths) from boundary  $\partial\Omega$ , we have*

$$\int_{\partial\Omega} \hat{\mathbf{G}}_{-a, \omega}^S(\mathbf{x}, \mathbf{y}) \overline{\hat{\mathbf{G}}_{a, \omega}^P(\mathbf{y}, \mathbf{z})} d\sigma(\mathbf{y}) \simeq \int_{\partial\Omega} \hat{\mathbf{G}}_{-a, \omega}^P(\mathbf{x}, \mathbf{y}) \overline{\hat{\mathbf{G}}_{a, \omega}^S(\mathbf{y}, \mathbf{z})} d\sigma(\mathbf{y}) \simeq 0. \quad (3.47)$$

### 3.4 Analysis of the regularized time-reversal imaging algorithm

The aim of this section is to justify that, in a homogeneous isotropic elastic medium, the regularized time-reversal imaging functional  $\tilde{\mathcal{J}}_{a, \rho}$  provides a correction of the attenuation effect.

**Theorem 3.6** *The regularized time-reversal imaging functional  $\tilde{\mathcal{I}}_{a,\rho}$  satisfies*

$$\tilde{\mathcal{I}}_{a,\rho}(\mathbf{x}) = \tilde{\mathcal{I}}_{\rho}(\mathbf{x}) + o(\varepsilon_S + \varepsilon_P), \tag{3.48}$$

$$\tilde{\mathcal{I}}_{\rho}(\mathbf{x}) := \int_{\partial\Omega} \int_0^T \left[ c_S \frac{\partial}{\partial s} \mathbf{G}^S(\mathbf{x}, \mathbf{y}, s) + c_P \frac{\partial}{\partial s} \mathbf{G}^P(\mathbf{x}, \mathbf{y}, s) \right] S_{\rho} [\mathbf{g}(\mathbf{y}, \cdot)](s) ds d\sigma(\mathbf{y}), \tag{3.49}$$

where  $S_{\rho}$  is defined by (3.12).

**Proof** We can decompose the functional  $\tilde{\mathcal{I}}_{a,\rho}$  as follows:

$$\begin{aligned} \tilde{\mathcal{I}}_{a,\rho}(\mathbf{x}) &= - \int_{\partial\Omega} \int_0^T \frac{\partial}{\partial s} [c_P \mathbf{G}_{-a,\rho}^P(\mathbf{x}, \mathbf{y}, T-s) + c_S \mathbf{G}_{-a,\rho}^S(\mathbf{x}, \mathbf{y}, T-s)] \mathbf{g}_a(\mathbf{y}, T-s) ds d\sigma(\mathbf{y}) \\ &= \int_{\partial\Omega} \int_0^T \frac{\partial}{\partial s} [c_P \mathbf{G}_{-a,\rho}^P(\mathbf{x}, \mathbf{y}, s) + c_S \mathbf{G}_{-a,\rho}^S(\mathbf{x}, \mathbf{y}, s)] [\mathbf{g}_a^S(\mathbf{y}, s) + \mathbf{g}_a^P(\mathbf{y}, s)] ds d\sigma(\mathbf{y}) \\ &= \mathcal{I}_{a,\rho}^{SS}(\mathbf{x}) + \mathcal{I}_{a,\rho}^{SP}(\mathbf{x}) + \mathcal{I}_{a,\rho}^{PS}(\mathbf{x}) + \mathcal{I}_{a,\rho}^{PP}(\mathbf{x}), \end{aligned}$$

where

$$\mathcal{I}_{a,\rho}^{\alpha\beta}(\mathbf{x}) = \int_{\partial\Omega} \int_0^T \frac{\partial}{\partial s} [c_{\alpha} \mathbf{G}_{-a,\rho}^{\alpha}(\mathbf{x}, \mathbf{y}, s)] \mathbf{g}_a^{\beta}(\mathbf{y}, s) ds d\sigma(\mathbf{y}), \quad \alpha, \beta \in \{P, S\}.$$

Similarly, we can decompose the functional  $\tilde{\mathcal{I}}_{\rho}$  as

$$\tilde{\mathcal{I}}_{\rho}(\mathbf{x}) = \mathcal{I}_{\rho}^{SS}(\mathbf{x}) + \mathcal{I}_{\rho}^{SP}(\mathbf{x}) + \mathcal{I}_{\rho}^{PS}(\mathbf{x}) + \mathcal{I}_{\rho}^{PP}(\mathbf{x}),$$

with

$$\mathcal{I}_{\rho}^{\alpha\beta}(\mathbf{x}) = \int_{\partial\Omega} \int_0^T \frac{\partial}{\partial s} [c_{\alpha} \mathbf{G}^{\alpha}(\mathbf{x}, \mathbf{y}, s)] S_{\rho} [\mathbf{g}^{\beta}(\mathbf{y}, \cdot)](s) ds d\sigma(\mathbf{y}), \quad \alpha, \beta \in \{P, S\}.$$

The first term  $\mathcal{I}_{a,\rho}^{SS}(\mathbf{x})$  satisfies

$$\begin{aligned} \mathcal{I}_{a,\rho}^{SS}(\mathbf{x}) &= \int_{\partial\Omega} \int_0^T \mathcal{A}_{-\varepsilon_S, \rho} \left[ \frac{\partial}{\partial s} [c_S \mathbf{G}^S(\mathbf{x}, \mathbf{y}, \cdot)] \right] (s) \mathcal{A}_{\varepsilon_S} [\mathbf{g}^S(\mathbf{y}, \cdot)](s) ds d\sigma(\mathbf{y}) \\ &= \int_{\partial\Omega} \int_0^T \frac{\partial}{\partial s} [c_S \mathbf{G}^S(\mathbf{x}, \mathbf{y}, s)] \mathcal{A}_{-\varepsilon_S, \rho}^* [\mathcal{A}_{\varepsilon_S} [\mathbf{g}^S(\mathbf{y}, \cdot)]](s) ds d\sigma(\mathbf{y}) \\ &= \int_{\partial\Omega} \int_0^T \frac{\partial}{\partial s} [c_S \mathbf{G}^S(\mathbf{x}, \mathbf{y}, s)] S_{\rho} [\mathbf{g}^S(\mathbf{y}, \cdot)](s) ds d\sigma(\mathbf{y}) + o(\varepsilon_S) \\ &= \mathcal{I}_{\rho}^{SS}(\mathbf{x}) + o(\varepsilon_S) \end{aligned}$$

by using Proposition 3.2. Similarly, we get

$$\mathcal{I}_{a,\rho}^{PP}(\mathbf{x}) = \mathcal{I}_{\rho}^{PP}(\mathbf{x}) + o(\varepsilon_P).$$

Moreover, the coupling terms  $\mathcal{J}_{a,\rho}^{SP}$  and  $\mathcal{J}_{a,\rho}^{PS}$  vanish. Indeed, thanks to Proposition 3.5, we have

$$\mathcal{J}_{a,\rho}^{SP}(\mathbf{x}) = \frac{1}{2\pi} \int_{\mathbb{R}^d} \int_{|\omega|<\rho} \omega^2 \left[ \int_{\partial\Omega} \left[ c_S \hat{\mathbf{G}}_{-a,\omega}^S(\mathbf{x}, \mathbf{y}) \right] \overline{\hat{\mathbf{G}}_{a,\omega}^P(\mathbf{y}, z)} d\sigma(\mathbf{y}) \right] d\omega \mathbf{F}(z) dz \simeq 0,$$

and

$$\mathcal{J}_{a,\rho}^{PS}(\mathbf{x}) = \frac{1}{2\pi} \int_{\mathbb{R}^d} \int_{|\omega|<\rho} \omega^2 \left[ \int_{\partial\Omega} \left[ c_P \hat{\mathbf{G}}_{-a,\omega}^P(\mathbf{x}, \mathbf{y}) \right] \overline{\hat{\mathbf{G}}_{a,\omega}^S(\mathbf{y}, z)} d\sigma(\mathbf{y}) \right] d\omega \mathbf{F}(z) dz \simeq 0.$$

Proposition 2.5 shows that we also have

$$\mathcal{J}_{\rho}^{SP}(\mathbf{x}) = \frac{1}{2\pi} \int_{\mathbb{R}^d} \int_{|\omega|<\rho} \omega^2 \left[ \int_{\partial\Omega} \left[ c_S \hat{\mathbf{G}}_{\omega}^S(\mathbf{x}, \mathbf{y}) \right] \overline{\hat{\mathbf{G}}_{\omega}^P(\mathbf{y}, z)} d\sigma(\mathbf{y}) \right] d\omega \mathbf{F}(z) dz \simeq 0,$$

$$\mathcal{J}_{\rho}^{PS}(\mathbf{x}) = \frac{1}{2\pi} \int_{\mathbb{R}^d} \int_{|\omega|<\rho} \omega^2 \left[ \int_{\partial\Omega} \left[ c_P \hat{\mathbf{G}}_{\omega}^P(\mathbf{x}, \mathbf{y}) \right] \overline{\hat{\mathbf{G}}_{\omega}^S(\mathbf{y}, z)} d\sigma(\mathbf{y}) \right] d\omega \mathbf{F}(z) dz \simeq 0,$$

which concludes the proof. □

It is straightforward to check that

$$\tilde{\mathcal{J}}_{\rho}(\mathbf{x}) \xrightarrow{\rho \rightarrow \infty} \tilde{\mathcal{J}}(\mathbf{x}) \simeq \mathbf{F}(\mathbf{x}) \tag{3.50}$$

by Theorem 2.6. Therefore,  $\tilde{\mathcal{J}}_{a,\rho}$  provides a first-order correction in terms of  $\varepsilon_S + \varepsilon_P$  of the attenuation effect. Moreover, the imaging functional  $\tilde{\mathcal{J}}_{a,\rho}$  can be seen as the time-reversal functional  $\tilde{\mathcal{J}}$  defined by (2.7) applied to  $\mathcal{A}_{-\varepsilon,\rho}^* \mathbf{g}_a^z, \alpha = P, S$ . As shown in (3.38), the regularized operator  $\mathcal{A}_{-\varepsilon,\rho}^*$  gives a first-order approximation of the inverse of  $\mathcal{A}_{\varepsilon}$ . It would be very interesting to construct higher order reconstructions in terms of the attenuation effect using higher order approximations of the inverse of operator  $\mathcal{A}_{\varepsilon}$ . The problem is more challenging than the one in the scalar case [5] because of the coupling between the shear and pressure components. Also note that if one applies the time-reversal functional  $\tilde{\mathcal{J}}$  to the data  $\mathbf{g}_a$  directly, then one finds

$$\begin{aligned} \tilde{\mathcal{J}}(\mathbf{x}) &= \int_{\partial\Omega} \int_0^T \frac{\partial}{\partial s} \left[ c_P \mathbf{G}^P(\mathbf{x}, \mathbf{y}, s) + c_S \mathbf{G}^S(\mathbf{x}, \mathbf{y}, s) \right] [\mathbf{g}_a(\mathbf{y}, \cdot)](s) ds d\sigma(\mathbf{y}) \\ &= \frac{1}{2\pi} \int_{\mathbb{R}^d} \int_{\mathbb{R}} \omega^2 \left[ \int_{\partial\Omega} \left[ c_P \hat{\mathbf{G}}_{\omega}^P(\mathbf{x}, \mathbf{y}) + c_S \hat{\mathbf{G}}_{\omega}^S(\mathbf{x}, \mathbf{y}) \right] \overline{\hat{\mathbf{G}}_{a,\omega}(\mathbf{y}, z)} d\sigma(\mathbf{y}) \right] d\omega \mathbf{F}(z) dz, \end{aligned} \tag{3.51}$$

which gives an error of the order of  $\varepsilon_S + \varepsilon_P$  as can be seen from expansion (3.36).

**Remark 3.7** Finally, it is worth emphasizing that the choice of the cut-off parameter  $\rho$  is based on the trade-off between image resolution and stability. On the one hand,  $\rho$  must be selected large enough for good resolution. On the other hand, for the stability of the reconstruction, it is required not to be too large. In the acoustic case,  $1/\sqrt{\varepsilon \text{diam}(\Omega)}$  (with  $\varepsilon$  being the attenuation coefficient) serves as a threshold for  $\rho$  in order to ensure stability, where  $\text{diam}$  denotes the diameter [5]. A threshold cut-off frequency  $\rho$  in the elastic case can accordingly be  $1/\sqrt{\max(\varepsilon_S, \varepsilon_P) \text{diam}(\Omega)}$ .

### 3.5 Numerical simulations

In this section we present numerical illustrations and describe our algorithms for numerical resolution of the source problem to show that  $\tilde{\mathcal{F}}_{a,\rho}$  provides a better reconstruction than  $\tilde{\mathcal{F}}$ , where the attenuation effect was not taken into account.

#### 3.5.1 Description of the algorithm

In the expression of  $\tilde{\mathcal{F}}_{a,\rho}$ , the solution  $v_{s,a,\rho}(\mathbf{x}, t)$  is very difficult to obtain numerically. Therefore, we prefer to regularize the problem by truncating high-frequency components in space instead of time, in contrast with our theoretical analysis. In general, the choice of regularization in time or in space depends on the numerical method used for computing the solution. Since a Fourier spectral scheme is used here, regularizing in space is simpler than regularizing in time.

This can be seen as an approximation  $\tilde{v}_{s,a,\rho}(\mathbf{x}, t)$  of  $v_{s,a,\rho}(\mathbf{x}, t)$  defined as the solution of

$$\frac{\partial^2 \tilde{v}_{s,a,\rho}}{\partial t^2}(\mathbf{x}, t) - \mathcal{L}_{\lambda,\mu} \tilde{v}_{s,a,\rho}(\mathbf{x}, t) + \frac{\partial}{\partial t} \mathcal{L}_{\eta_\lambda, \eta_\mu} \tilde{v}_{s,a,\rho}(\mathbf{x}, t) = \frac{d\delta_s(t)}{dt} \mathcal{X}_\rho [g_a(\cdot, T - s)\delta_{\partial\Omega}](\mathbf{x})\delta_{\partial\Omega}(\mathbf{x}),$$

where the operator  $\mathcal{X}_\rho$  is defined by

$$\mathcal{X}_\rho [f](\mathbf{x}) = \int_{|\mathbf{k}| \leq \rho} \left[ \int_{\mathbb{R}^d} f(\mathbf{y}) \exp(-2i\pi\mathbf{k} \cdot \mathbf{y}) d\mathbf{y} \right] \exp(2i\pi\mathbf{k} \cdot \mathbf{x}) d\mathbf{k}.$$

The operator  $\mathcal{X}_\rho$ , as the operator  $S_\rho$ , truncates high frequencies but in the space variable. Note that a criteria for choosing  $\rho$  similar to the one in the case of a truncation in time can be obtained.

To compute the solution of the viscoelastic wave equation in two dimensions

$$\frac{\partial^2 \mathbf{u}_a}{\partial t^2}(\mathbf{x}, t) - \mathcal{L}_{\lambda,\mu} \mathbf{u}_a(\mathbf{x}, t) - \frac{\partial}{\partial t} \mathcal{L}_{\eta_\lambda, \eta_\mu} \mathbf{u}_a(\mathbf{x}, t) = \mathbf{0},$$

we use the same algorithm presented in the purely elastic case, i.e. we use a larger box  $\Omega \subset Q = [-L/2, L/2]^2$  with periodic boundary conditions and again a *splitting spectral Fourier* approach coupled with a PML technique to simulate a free outgoing interface on  $\partial Q$ .

#### 3.5.2 Experiments

In the sequel, for numerical illustrations,  $\Omega$  is taken to be a unit disc. Its boundary is discretized by  $2^{11}$  sensors. Each solution of elastic wave equation is computed over  $(\mathbf{x}, t) \in [-L/2, L/2]^2 \times [0, T]$  with  $L = 4$  and  $T = 2$ . The discretization steps are  $dt = T/2^{13}$  and  $dx = L/2^9$ .

Figure 4 presents the first experiment with Lamé parameters  $(\lambda, \mu) = (1, 1)$  and attenuation coefficients  $(\eta_\lambda, \eta_\mu) = (0.0002, 0.0002)$ , which gives  $(\varepsilon_P, \varepsilon_S) = (0.0002, 0.0002)$ . The first (top) line corresponds to the two components of the initial source  $\mathbf{F}$ . The second line corresponds to the reconstruction of  $\mathbf{F}$  without taking into account the attenuation

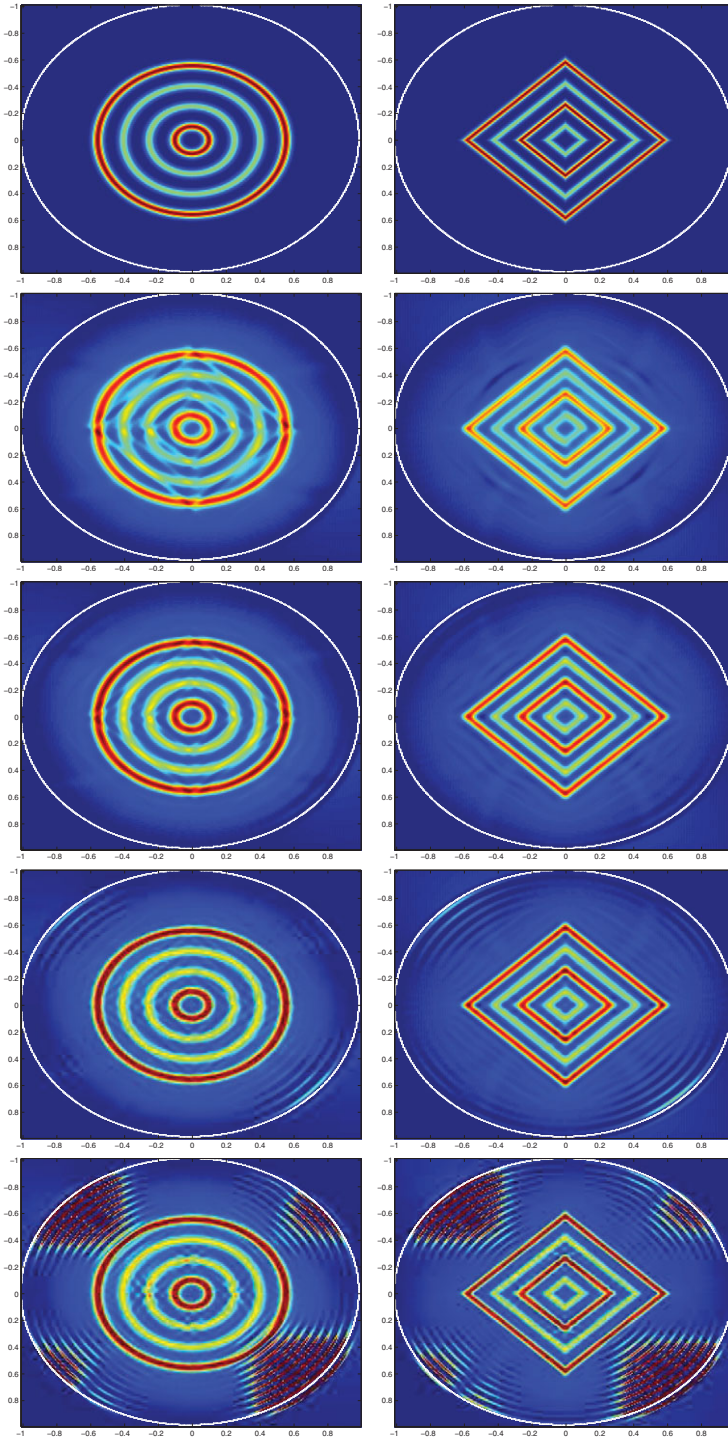


FIGURE 4. (Colour online) Comparison between  $\tilde{\mathcal{I}}$  and  $\tilde{\mathcal{I}}_{a,\rho}$  in a viscoelastic medium. The parameters are  $(\lambda, \mu) = (1, 1)$  and  $(\eta_\lambda, \eta_\mu) = (0.0002, 0.0002)$ . From top to bottom: initial source; second line: without correction of attenuation; last lines: with  $\tilde{\mathcal{I}}_{a,\rho}$  and  $\rho = 15, 20, 25$ .

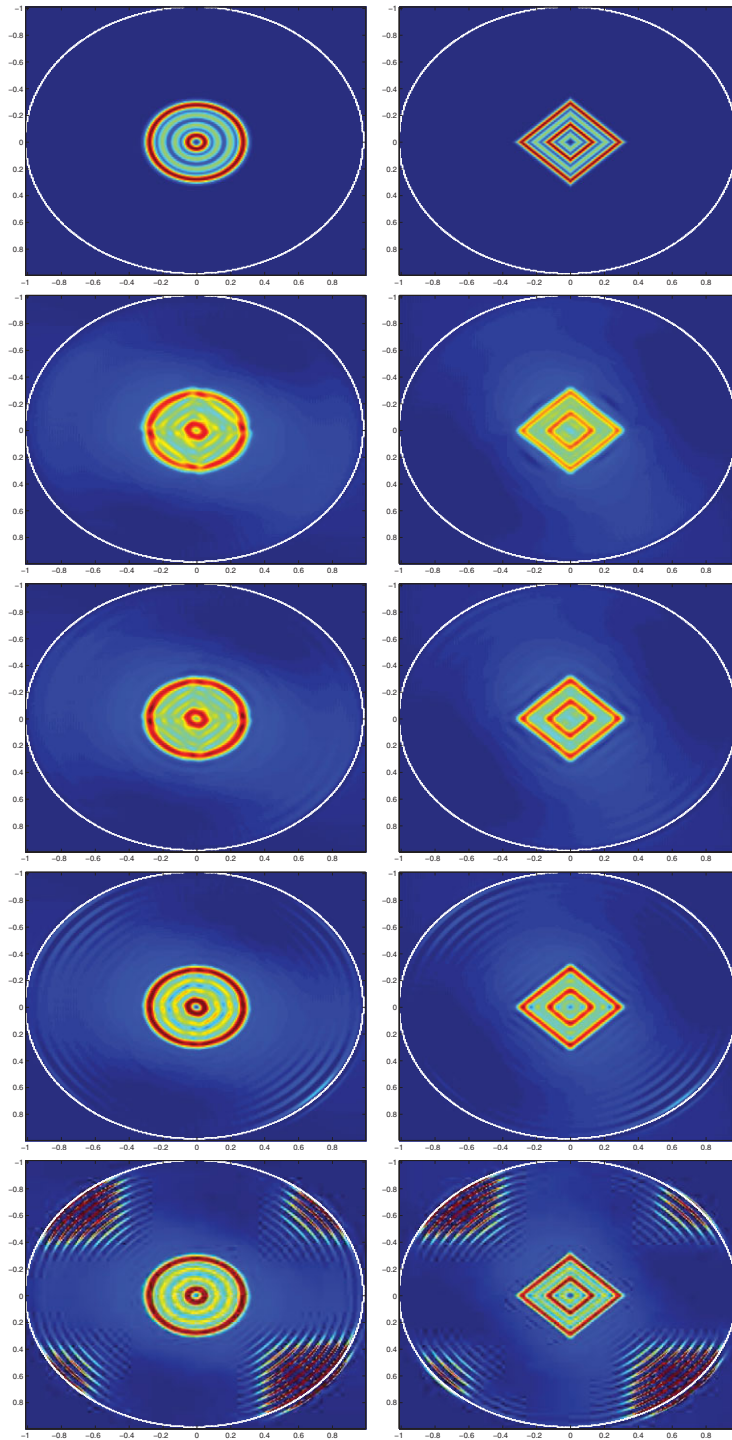


FIGURE 5. (Colour online) Comparison between  $\tilde{\mathcal{I}}$  and  $\tilde{\mathcal{I}}_{a,\rho}$  in a viscoelastic medium. The parameters are  $(\lambda, \mu) = (1, 1)$  and  $(\eta_\lambda, \eta_\mu) = (0.00005, 0.00005)$ . First line: initial source; second line: without correction of attenuation; last lines: with  $\tilde{\mathcal{I}}_{a,\rho}$  and  $\rho = 15, 20, 25$ .



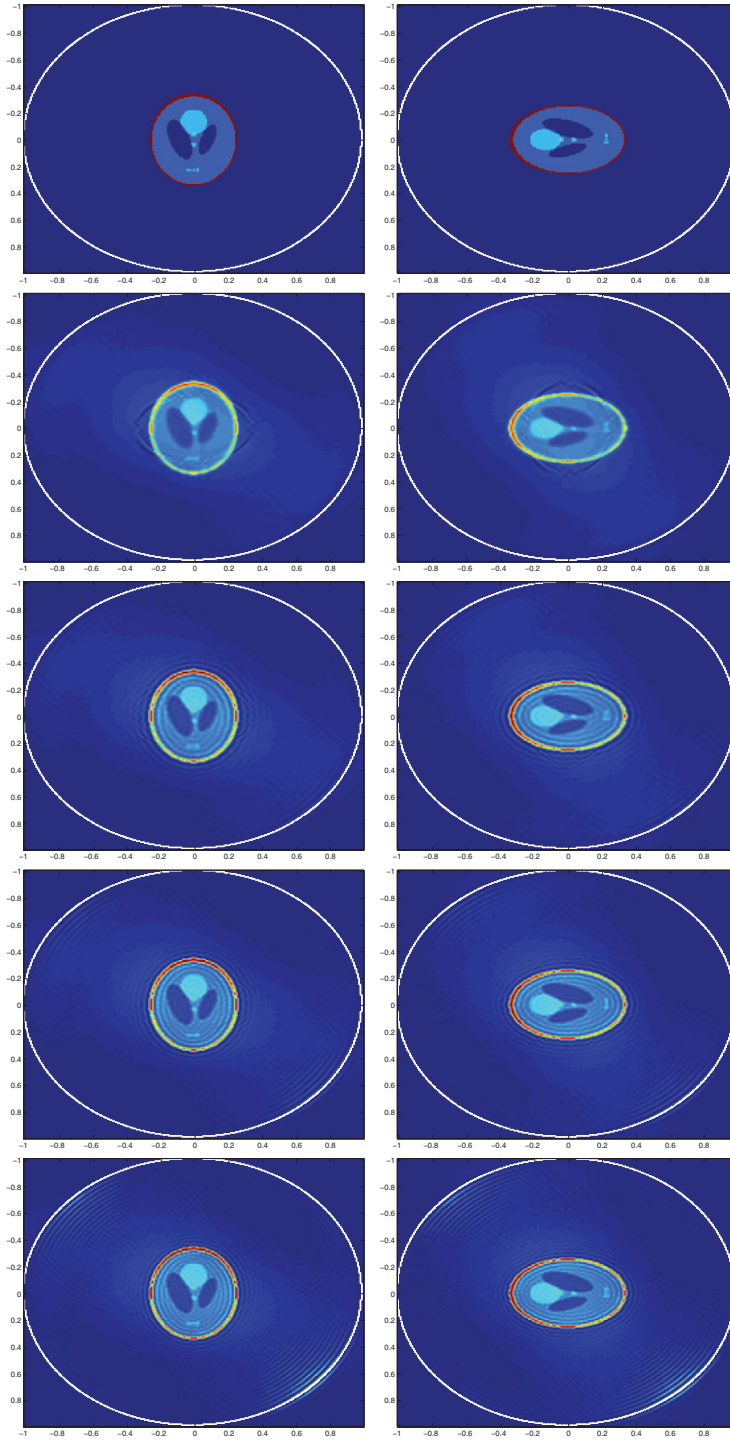


FIGURE 6. (Colour online) Comparison between  $\tilde{\mathcal{J}}$  and  $\tilde{\mathcal{J}}_{a,\rho}$  in a viscoelastic medium. The parameters are  $(\lambda, \mu) = (1, 1)$  and  $(\eta_\lambda, \eta_\mu) = (0.00005, 0.00005)$ . First line: initial source  $\mathbf{F}$ ; second line: reconstruction of  $\mathbf{F}$  using  $\tilde{\mathcal{J}}$ ; last three lines: reconstruction of  $\mathbf{F}$  using  $\tilde{\mathcal{J}}_{a,\rho}$  with  $\rho = 25, 30, 35$ .

effect. The imaging functional  $\tilde{\mathcal{I}}(\mathbf{x})$  appears to be blurred due to coupling effects. The last three lines correspond to the reconstructions of  $\mathbf{F}$  using the imaging functional  $\tilde{\mathcal{I}}_{a,\rho}$  with different values of  $\rho$ . We clearly observe a better reconstruction of the source  $\mathbf{F}$  using  $\tilde{\mathcal{I}}_{a,\rho}$  than using the functional  $\tilde{\mathcal{I}}$  provided that the regularization parameter  $\rho$  is chosen appropriately large to insure a good resolution of the reconstruction.

Figures 5 and 6 present two other examples of reconstruction using  $\tilde{\mathcal{I}}_{a,\rho}$ . The same observation holds.

### 4 Conclusion

In this paper, we have introduced fundamental tools for elastic wave imaging in both elastic and viscoelastic media. We have presented and analysed time-reversal algorithms based on a weighted Helmholtz decomposition that have significantly better focusing properties. We have proved new Kirchhoff–Helmholtz identities. We have numerically highlighted the potential of our original approach. We plan to use the analytical and numerical tools introduced in this paper to develop cross-correlation techniques for imaging in cluttered elastic media.

### Appendix A Proof of ((3.46)) and definition of attenuation operators

Let

$$\mathcal{L}_{\eta_\lambda, \eta_\mu}^S \mathbf{u} = c_S^2 \varepsilon_S [\Delta \mathbf{u} - \nabla(\nabla \cdot \mathbf{u})] \quad \text{and} \quad \mathcal{L}_{\eta_\lambda, \eta_\mu}^P \mathbf{u} = c_P^2 \varepsilon_P \nabla(\nabla \cdot \mathbf{u}), \tag{A 1}$$

where

$$\varepsilon_S = \frac{\eta_\mu}{\mu} \quad \text{and} \quad \varepsilon_P = \frac{\eta_\lambda + 2\eta_\mu}{\lambda + 2\mu}. \tag{A 2}$$

We have

$$(\mathcal{L}_{\lambda, \mu}^\alpha \mp i\omega \mathcal{L}_{\eta_\lambda, \eta_\mu}^\alpha + \omega^2) \hat{\mathbf{G}}_{\pm a, \omega}^\alpha(\mathbf{x}, \mathbf{y}) = \mathcal{H}^\alpha[-\delta_{\mathbf{y}} \mathbf{I}](\mathbf{x}), \quad \alpha = P, S. \tag{A 3}$$

Recall also that tensor  $\hat{\mathbf{G}}_{\pm a, \omega}^\alpha$  is the solution to (A 3). Moreover, from (A 1), we have

$$\mathcal{L}_{\eta_\lambda, \eta_\mu}^\alpha [\hat{\mathbf{G}}_{\pm a, \omega}^\alpha \mathbf{p}] = \varepsilon_\alpha \mathcal{L}_{\lambda, \mu}^\alpha [\hat{\mathbf{G}}_{\pm a, \omega}^\alpha \mathbf{p}] \quad \forall \mathbf{p} \in \mathbb{R}^d, \quad \alpha = P, S. \tag{A 4}$$

Therefore, by virtue of (A 3) and (A 4), we have for all  $\mathbf{x} \neq \mathbf{y}$

$$((1 \mp i\omega \varepsilon_\alpha) \mathcal{L}_{\lambda, \mu}^\alpha + \omega^2 \mathbf{I}) \hat{\mathbf{G}}_{\pm a, \omega}^\alpha(\mathbf{x}, \mathbf{y}) = \mathcal{H}^\alpha[-\delta_{\mathbf{y}} \mathbf{I}](\mathbf{x}),$$

or equivalently,

$$(\mathcal{L}_{\lambda, \mu}^\alpha + \kappa_{\pm \varepsilon_\alpha}(\omega)^2) \hat{\mathbf{G}}_{\pm a, \omega}^\alpha(\mathbf{x}, \mathbf{y}) = \frac{1}{1 \mp i\omega \varepsilon_\alpha} \mathcal{H}^\alpha[-\delta_{\mathbf{y}} \mathbf{I}](\mathbf{x}) = \left[ \frac{\kappa_{\pm \varepsilon_\alpha}(\omega)}{\omega} \right]^2 \mathcal{H}^\alpha[-\delta_{\mathbf{y}} \mathbf{I}](\mathbf{x}), \tag{A 5}$$

where

$$\kappa_{\pm \varepsilon}(\omega) = \frac{\omega}{\sqrt{1 \mp i\omega \varepsilon}}. \tag{A 6}$$

Note also that  $\widehat{\mathbf{G}}_\omega^\alpha$  satisfies, for all  $\mathbf{x} \neq \mathbf{y}$ ,

$$(\mathcal{L}_{\lambda,\mu}^\alpha + \omega^2) \widehat{\mathbf{G}}_\omega^\alpha(\mathbf{x}, \mathbf{y}) = \mathcal{H}^\alpha[-\delta_{\mathbf{y}}\mathbf{I}](\mathbf{x}), \quad \alpha = P, S, .$$

Consequently,

$$(\mathcal{L}_{\lambda,\mu}^\alpha + \kappa_{\pm\epsilon}(\omega)^2) \widehat{\mathbf{G}}_{\kappa_{\pm\epsilon}(\omega)}^\alpha(\mathbf{x}, \mathbf{y}) = \mathcal{H}^\alpha[-\delta_{\mathbf{y}}\mathbf{I}](\mathbf{x}), \quad \alpha = P, S. \tag{A 7}$$

Therefore, comparing (A 7) and (A 5) and using the argument of a unique solution subject to radiation conditions, we conclude that

$$\widehat{\mathbf{G}}_{\pm a,\omega}^\alpha(\mathbf{x}, \mathbf{y}) = \left[ \frac{\kappa_{\pm\epsilon_x}(\omega)}{\omega} \right]^2 \widehat{\mathbf{G}}_{\kappa_{\pm\epsilon_x}(\omega)}^\alpha(\mathbf{x}, \mathbf{y}), \quad \alpha = P, S. \tag{A 8}$$

In particular, as  $\widehat{\mathbf{u}}_\omega^\alpha$  and  $\widehat{\mathbf{u}}_{a,\omega}^\alpha$ , respectively, satisfy

$$(\omega^2 + \mathcal{L}_{\lambda,\mu}^\alpha) \widehat{\mathbf{u}}_\omega^\alpha = i\omega \mathcal{H}^\alpha[\mathbf{F}] \quad \text{and} \quad (\kappa_{\epsilon_x}(\omega)^2 + \mathcal{L}_{\lambda,\mu}^\alpha) \widehat{\mathbf{u}}_{a,\omega}^\alpha = i \frac{\kappa_{\epsilon_x}(\omega)^2}{\omega} \mathcal{H}^\alpha[\mathbf{F}], \quad \alpha = P, S, \tag{A 9}$$

we have

$$\widehat{\mathbf{u}}_{a,\omega}^\alpha(\mathbf{x}) = \frac{\kappa_{\epsilon_x}(\omega)}{\omega} \widehat{\mathbf{u}}_{\kappa_{\epsilon_x}(\omega)}^\alpha(\mathbf{x}). \tag{A 10}$$

Consequently, by using inverse Fourier transform, we arrive at

$$\mathbf{u}_a^\alpha = \mathcal{A}_{\epsilon_x}[\mathbf{u}^\alpha], \tag{A 11}$$

where the attenuation operator  $\mathcal{A}_\epsilon$ , for  $\epsilon > 0$ , is given by

$$\mathcal{A}_\epsilon[\phi](t) = \frac{1}{2\pi} \int_{\mathbb{R}} \frac{\kappa_\epsilon(\omega)}{\omega} \left\{ \int_{\mathbb{R}^+} \phi(s) \exp\{i\kappa_\epsilon(\omega)s\} ds \right\} \exp\{-i\omega t\} d\omega, \quad t > 0. \tag{A 12}$$

### References

- [1] AKI, K. & RICHARDS, P. G. (1980) *Quantitative Seismology, Vol. 1*, W. H. Freeman, San Francisco, CA.
- [2] AMMARI, H. (2008) *An Introduction to Mathematics of Emerging Biomedical Imaging, Mathematics & Applications, Vol. 62*, Springer-Verlag, Berlin, Germany.
- [3] AMMARI, H., ASCH, M., JUGNON, V., GUADARRAMA BUSTOS, L. & KANG, H. (2011) Transient imaging with limited-view data. *SIAM J. Imaging Sci.* **4**, 1097–1121.
- [4] AMMARI, H., BOSSY, E., JUGNON, V. & KANG, H. (2010) Mathematical modelling in photoacoustic imaging of small absorbers. *SIAM Rev.* **52**, 677–695.
- [5] AMMARI, H., BRETIN, E., GARNIER, J. & WAHAB, A. (2011) Time reversal in attenuating acoustic media. In: *Mathematical and Statistical Methods for Imaging*, Contemporary Mathematics series, Vol. 548, American Mathematical Society, Providence, RI, pp. 151–163.
- [6] AMMARI, H., BRETIN, E., GARNIER, J. & WAHAB, A. (2012) Noise source localization in an attenuating medium. *SIAM J. Appl. Math.* **72**, 317–336.
- [7] AMMARI, H., BRETIN, E., JUGNON, V. & WAHAB, A. (2011) Photoacoustic imaging for attenuating acoustic media. In: *Mathematical Modeling in Biomedical Imaging II*, Lecture Notes in Mathematics, Vol. 2035, Springer-Verlag, Berlin, Germany, pp. 57–84.

- [8] AMMARI, H., CAPDEBOSCO, Y., KANG, H. & KOZHEMYAK, A. (2009) Mathematical models and reconstruction methods in magneto-acoustic imaging. *Euro. J. Appl. Math.* **20**, 303–317.
- [9] AMMARI, H., GARAPON, P., GUADARRAMA BUSTOS, L. & KANG, H. (2010) Transient anomaly imaging by the acoustic radiation force. *J. Diff. Equ.* **249**, 1579–1595.
- [10] AMMARI, H., GARAPON, P., KANG, H. & LEE, H. (2008) A method of biological tissues elasticity reconstruction using magnetic resonance elastography measurements. *Quart. Appl. Math.* **66**, 139–175.
- [11] AMMARI, H., GUADARRAMA-BUSTOS, L., KANG, H. & LEE, H. (2011) Transient elasticity imaging and time reversal. *Proc. R. Soc. Edinburgh Math.* **141**, 1121–1140.
- [12] AMMARI, H. & KANG, H. (2007) *Polarization and Moment Tensors: With Applications to Inverse Problems and Effective Medium Theory*, Applied Mathematical Sciences series, Vol. 162, Springer-Verlag, New York.
- [13] BERCOFF, J., TANTER, M., MULLER, M. & FINK, M. (2004) The role of viscosity in the impulse diffraction field of elastic waves induced by the acoustic radiation force. *IEEE Trans. Ultrason. Ferro. Freq. Control* **51**, 1523–1536.
- [14] BORCEA, L., PAPANICOLAOU, G. & TSOGKA, C. (2003) Theory and applications of time reversal and interferometric imaging. *Inverse Probl.* **19**, 134–164.
- [15] BORCEA, L., PAPANICOLAOU, G. & TSOGKA, C. (2005) Interferometric array imaging in clutter. *Inverse Probl.* **21**, 1419–1460.
- [16] BORCEA, L., PAPANICOLAOU, G., TSOGKA, C. & BERRYMAN, J. G. (2002) Imaging and time reversal in random media. *Inverse Probl.* **18**, 1247–1279.
- [17] BRETIN, E., GUADARRAMA BUSTOS, L. & WAHAB, A. (2011) On the Green function in visco-elastic media obeying a frequency power-law. *Math. Meth. Appl. Sci.* **34**, 819–830.
- [18] CANUTO, C., HUSSAINI, M. Y., QUARTERONI, A. & ZANG, T. A. (1987) *Spectral Methods in Fluid Dynamics*, Springer-Verlag, New York.
- [19] CATHELIN, S., BENECH, N., BRUM, J. & NEGREIRA, C. (2008) Time-reversal of elastic waves in soft solids. *Phys. Rev. Lett.* **100**, 064301.
- [20] CATHELIN, S., GENNISSON, J. L., DELON, G., SINKUS, R., FINK, M., ABDOUELKARAM, S. & CULIOLI, J. (2004) Measurement of visco-elastic properties of solid using transient elastography: An inverse problem approach. *J. Acous. Soc. Am.* **116**, 3734–3741.
- [21] CHEN, Z. & ZHANG, X. (preprint) An anisotropic perfectly matched layer method for three-dimensional elastic scattering problems.
- [22] DE ROSNY, J., LEROSEY, G., TOURIN, A. & FINK, M. (2007) Time reversal of electromagnetic waves. In: *Lecture Notes in Computer Science and Engineering*, Vol. 59, Springer-Verlag, New York.
- [23] FINK, M. (1997) Time-reversed acoustics. *Phys. Today* **50**, 34.
- [24] FINK, M. & PRADA, C. (2001) Acoustic time-reversal mirrors. *Inverse Probl.* **17**, R1–R38.
- [25] FOUQUE, J.-P., GARNIER, J. & NACHBIN, A. (2004) Time reversal for dispersive waves in random media. *SIAM J. Appl. Math.* **64**, 1810–1838.
- [26] FOUQUE, J.-P., GARNIER, J., NACHBIN, A. & SØLNA, K. (2005) Time reversal refocusing for point source in randomly layered media. *Wave Motion* **42**, 238–260.
- [27] FOUQUE, J.-P., GARNIER, J., PAPANICOLAOU, G. & SØLNA, K. (2007) *Wave Propagation and Time Reversal in Randomly Layered Media*, Springer, New York.
- [28] FOUQUE, J.-P., GARNIER, J. & SØLNA, K. (2006) Time reversal super resolution in randomly layered media. *Wave Motion* **43**, 646–666.
- [29] GALDI, G. P. (1994) *An Introduction to the Mathematical Theory of the Navier-Stokes Equations, Vol. I, Linearized Steady Problems*, Springer-Verlag, New York.
- [30] GREENLEAF, J. F., FATEMI, M. & INSANA, M. (2003) Selected methods for imaging elastic properties of biological tissues. *Annu. Rev. Biomed. Eng.* **5**, 57–78.
- [31] HASTINGS, F., SCHNEIDER, J. B. & BROCHAT, S. L. (1996) Application of the perfectly matched layer (PML) absorbing boundary condition to elastic wave propagation. *J. Acoust. Soc. Am.* **100**, 3061–3069.

- [32] HÖRMANDER, L. (2003) *The Analysis of Linear Partial Differential Operators. I. Distribution Theory and Fourier Analysis*, Classics in Mathematics, Springer-Verlag, Berlin, Germany.
- [33] KALIMERIS, K. & SCHERZER, O. (to appear) Photoacoustic imaging in attenuating acoustic media based on strongly causal models. *Math. Meth. Appl. Sci.* (arXiv:1211.1516v1) doi:10.1002/mma.2756.
- [34] KOWAR, R. & SCHERZER, O. (2011) Photoacoustic imaging taking into account attenuation. In: *Mathematical Modeling in Biomedical Imaging II*, Lecture Notes in Mathematics, Vol. 2035, Springer-Verlag, Berlin, Germany, pp. 85–130.
- [35] KOWAR, R., SCHERZER, O. & BONNEFOND, X. (2011) Causality analysis of frequency dependent wave attenuation. *Math. Meth. Appl. Sci.* **34**, 108–124.
- [36] LARMAT, C., MONTAGNER, J. P., FINK, M., CAPDEVILLE, Y., TOURIN, A. & CLÉVÉDÉ, E. (2006) Time-reversal imaging of seismic sources and application to the great Sumatra earthquake. *Geophys. Res. Lett.* **33**, L19312.
- [37] LEROSEY, G., DE ROSNY, J., TOURIN, A., DERODE, A., MONTALDO, G. & FINK, M. (2005) Time-reversal of electromagnetic waves and telecommunication. *Radio Sci.* **40**, RS6S12.
- [38] NÄSHOLM, S. P. & HOLM, S. (2013) On a fractional zener elastic wave equation. *Fract. Calcul. Appl. Anal.* **16**, 26–50.
- [39] NORVILLE, P. D. & SCOTT, W. R. (2005) Time-reversal focusing of elastic surface waves. *J. Acoust. Soc. Am.* **118**, 735–744.
- [40] PHUNG, K. D. & ZHANG, X. (2008) Time reversal focusing of the initial state for Kirchhoff plate. *SIAM J. Applied Math.* **68**, 1535–1556.
- [41] PRADA, C., KERBRAT, E., CASSEREAU, D. & FINK, M. (2002) Time reversal techniques in ultrasonic nondestructive testing of scattering media. *Inverse Probl.* **18**, 1761–1773.
- [42] PUJOL, J. (2003) *Elastic Wave Propagation and Generation in Seismology*, Cambridge University Press, Cambridge, UK.
- [43] SARVAZAN, A. P., RUDENKO, O. V., SWANSON, S. C., FOWLKERS, J. B. & EMELIANOV, S. V. (1998) Shear wave elasticity imaging: A new ultrasonic technology of medical diagnostics. *Ultrasound Med. Biol.* **24**, 1419–1435.
- [44] STRANG, G. (1968) On the construction and comparison of difference schemes. *SIAM J. Numer. Anal.* **5**, 506–517.
- [45] SZABO, T. L. AND WU, J. A model for longitudinal and shear wave propagation in viscoelastic media. *J. Acous. Soc. Am.* **107**, 2437–2446.
- [46] TANTER, M. AND FINK, M. Time reversing waves for biomedical Applications, In: *Mathematical Modeling in Biomedical Imaging I*, Lecture Notes in Mathematics vol. 1983, Springer-Verlag, 2009, pp. 73–97.
- [47] TENG, J. J., ZHANG, G. & HUANG, S. X. (2007) Some theoretical problems on variational data assimilation. *Appl. Math. Mech.* **28**, 581–591.
- [48] WAPENAAR, K. (2004) Retrieving the elastodynamic Green’s function of an arbitrary inhomogeneous medium by cross correlation. *Phys. Rev. Lett.* **93**, 254301.
- [49] WAPENAAR, K. & FOKKEMA, J. (2006) Green’s function representations for seismic interferometry. *Geophysics* **71**, S133–S146.
- [50] WIEGMANN, A. (June 1999), *Fast Poisson, Fast Helmholtz and Fast Linear Elastostatic Solvers on Rectangular Parallelepipeds*. Technical Report LBNL-43565, Lawrence Berkeley National Laboratory, Berkeley CA.
- [51] XU, Y. & WANG, L. V. (2004) Time reversal and its application to tomography with diffraction sources. *Phys. Rev. Lett.* **92**, 033902.